 doi:10.20944/preprints202103.0642.v1

Article

On the use of NB-IoT over GEO satellite systems with time-packed optical feeder links for over-the-air firmware/software updates of machine-type terminals

Joan Bas[1]* and Alexis A. Dowhuszko[2]

[1] Department of Array and Multi-Sensor Processing, Centre Tecnològic de Telecomunicacions de Catalunya (CTTC/CERCA), Castelldefels (Barcelona), Spain
[2] Department of Communications and Networking, Aalto University, 02150 Espoo, Finland
E-mails: joan.bas@cttc.es; alexis.dowhuszko@aalto.fi
* Correspondence: Av. Karl Friedriech Gauss 7 - Building B4, 08860 Castelldefels, Spain. Tel.: +34 93 645 29 12

Abstract: The verticals of 5G, such as the automotive, smart grid and smart cities sectors, will bring lots of new sensors and IoT devices requiring Internet connectivity. Most of these machine-type terminals will be sparsely distributed, covering a very large geographical area and, from time to time, will have to update their software, firmware and/or other relevant data. Given this situation, one viable solution to implement the *"Over-the-Air"* update of these IoT terminals can be with the aid of GEO satellite systems. However, due to the ultra-dense radio frequency reuse that contemporary High-Throughput Satellite (HTS) systems implement in the *access link* to serve the IoT terminals, the use of a time-packed Free Space Optical (FSO) link represents a practical solution to avoid the bottleneck that the satellite gateway experiences in the *feeder link*. The performance of both *Detect-and-Forward* and *Decode-and-Forward* relaying strategies are studied, assuming that the single-carrier M-PAM symbols that are transmitted on the optical feeder link are mapped into M-QAM symbols that modulate the multiple subcarriers of the OFDM-based radio access link. In addition, the benefits of encapsulating the NB-IoT frames into DVB-S2(X) satellite frames is also analyzed in detail. The effects of the impairments introduced in both optical feeder and radio access links are characterized in detail, and the end-to-end error correction capabilities of the Modulation and Coding Schemes (MCS) defined in the contemporary releases of the NB-IoT and DVB-S2(X) standards are studied for different working regimes.

Keywords: NB-IoT; DVB-S2(X); High-Throughput Satellite; Optical Feeder Link; Over-the-air updates; Time-Packing; Decode-and-Forward; Scintillation; Beam-Wander; Convolutional Coding.

1. Introduction

In the forthcoming years, an increased data rate capacity will be needed to provide enhanced Mobile Broadband (eMBB) and massive Machine-Type Communications (mMTC) fueled, among other reasons, by the large demand of video transmissions and IoT communications that that are foreseen in future vertical services [1]. Specifically, according to CISCO, it is expected that Machine-to-Machine (M2M) connections will reach 14.7 billions by 2023. Applications such as home automation, home security, video surveillance, connected white goods and tracking will represent practically the half of the total M2M connections by 2023 [2]. Furthermore, the M2M services that are experiencing fastest growth in these days are connected car applications, such as fleet management, in-vehicle entertainment, emergency calling, vehicle diagnostics and navigation, with a Compound Annual Growing Rate (CAGR) in the order of 30%. All these applications share the same requirement,

 doi:10.20944/preprints202103.0642.v1

known as Over-The-Air (OTA) programming, to update the software (*e.g.*, maps for navigation), security keys (*e.g.*, for cryptography in the IoT devices), among other firmware updates.

In practical terms, the foreseen growth of OTA applications implies that the downlink channel (*i.e.*, from the base station to the IoT terminals) will have to be improved to support the expected data traffic demand. Furthermore, given that Machine-type terminals may be sparsely deployed in large geographical areas, then the use of satellite network would be an excellent option to enable reliable IoT connectivity in a global scale. Towards this regard, the advent of Very High Throughput Satellite (VHTS) systems will permit satellite operators to achieve a total network capacity of few Terabits-per-second [3,4]. In this process, the use of optical technology complemented by spectral efficient techniques can play a key role to reduce the bottleneck that represents the VHTS feeder link.

The design of the optical feeder link depends on the approach that the GEO satellite uses to forward the information that receives from the satellite gateway [5]. In the *"ideal"* case of a GEO satellite that implements a fully regenerative payload, the optical feeder link would be terminated in the satellite, and a robust modulation and coding scheme could be selected to address the bit error bursts that the turbulent optical satellite wireless channel introduce [6]. In the transparent non-regenerative *"bent-pipe"* solutions, on the other hand, the instantaneous value of the radio signal is used to modulate the intensity of the optical carrier of the feeder link Laser Diode (LD) with the aid of an external Match-Zehnder Modulator (MZM) [7]. Moreover, if time-packing encoding is applied on the real-valued electrical signal that is used to modulate the intensity of the LD beam, the data throughput of the optical feeder link can be increased even further, without the necessity of using a wider communication bandwidth. This effect is obtained by shrinking the separation between adjacent transmitted pulses [8], mitigating part of the Inter-Symbol Interference (ISI) power that time-packing introduces with the aid of a linear equalizer that is placed on-board the GEO satellite before symbol detection [9]. It is important to highlight that the impact of the residual ISI, which remains in the forward link after the GEO satellite relaying, can be further mitigated with the proper selection of the Modulation and Coding Schemes (MCS) to communication with the NB-IoT terminal [10].

The forward link of a satellite system can be divided into two parts, namely: i) The optical feeder link (uplink), from the ground station to the GEO satellite, and ii) the radio access link (downlink), from the GEO satellite to the NB-IoT user terminals. Therefore, and in order to improve the achievable throughput of the forward direction of communication of the GEO satellite system under different working conditions, we study in this paper three different relaying architectures, namely: 1) *Detect-and-Forward* (non-regenerative strategy), where the GEO satellite only detects the symbols of the NB-IoT frames that modulate the intensity of the optical beam, and forwards them to the NB-IoT devices after M-PAM to M-QAM mapping; 2) *Decode-and-Forward with NB-IoT* (regenerative strategy), where the GEO satellite detects and decodes the symbols of the NB-IoT frames that are transported on the optical feeder link, and forwards them to the IoT devices after the NB-IoT frame regeneration for downlink radio transmission; and finally, 3) *Decode-and-Forward with NB-IoT/DVB-S2(X)* (regenerative strategy), where the NB-IoT frames are encapsulated into DVB-S2(X) satellite frames for uplink transmission and, in the GEO satellite, the DVB-S2(X) decoding is performed to recover the NB-IoT frame that is then transmitted to the NB-IoT terminals.

The remaining part of this article has been structured as follows: Section 2 summarizes the key concepts to model the MCS defined in the NB-IoT standard, the three proposed relaying architectures using GEO satellites with optical feeder links (one non-regenerative and two regenerative), and the details of the time-packing equalization and low-complexity Log Likelihood Ratio (LLR) computation for soft decoding. Section 3 studies the effect of the turbulent atmosphere in the optical feeder link, with emphasis on the beam wander and scintillation that is introduced in the uplink transmission. Section 4 presents the simulation setup and the performance figures in terms of end-to-end Block Error Rate (BLER) and throughput. Finally, conclusions are drawn in Section 5.

Preprints (www.preprints.org) | NOT PEER-REVIEWED | Posted: 25 March 2021 doi:10.20944/preprints202103.0642.v1

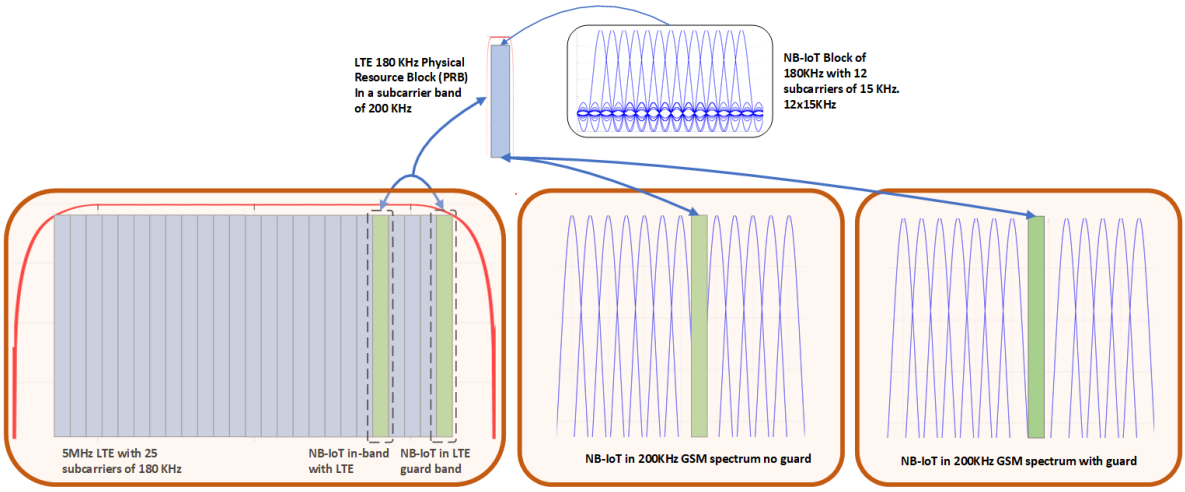

Figure 1. *Typologies of NB-IoT deployment, namely stand-alone, in-band and guard-band deployments. All these deployment configurations are compatible with the channelization that is used in contemporary mobile communication standards, such as GSM/2G (200 kHz channel) and LTE/4G (180 kHz Physical Resource Block).*

2. System Model

This section summarizes the key technological concepts that are needed to model the link level performance of the NB-IoT communication, as well as the different relaying architectures that could be used on-board the GEO satellite to interface the optical wireless signal (uplink) into the radio wireless signal (downlink) that is forwarded from the GEO satellite to the NB-IoT terminals.

2.1. NB-IoT signal format for the satellite forward link

NB-IoT has been developed by 3GPP to cope with the large demand on IoT connectivity that is foreseen by the designers of the future generations of mobile communications standards (*i.e.*, 5G and beyond). NB-IoT has been conceived to be deployed in three different configurations or typologies, which are compatible with the spectrum allocation (channelization) that is used in contemporary mobile communication standards such as GSM (2G) and LTE (4G). An overview of these deployment typologies, which are known as *stand-alone*, *in-band* and *guard-band*, can be appreciated in Fig. 1.

In the stand-alone deployment, the NB-IoT signal occupies the bandwidth that corresponds to one (or few) of the 200 kHz GSM radio channels of the 2G radio spectrum; note that this strategy is suitable for the re-farming process of GSM bands. In the in-band deployment, the NB-IoT signal is placed on the radio spectrum that corresponds to one (or few) Physical Resource Blocks (PRB) of an LTE carrier, where each PRB spans over 180 kHz of bandwidth and it is formed by 12 sub-carriers of 15 kHz bandwidth each. Finally, in the third typology of deployment known as guard-band deployment, the NB-IoT signal is placed on the guard bands that are reserved to prevent adjacent-channel interference between LTE carriers. Note that these strategies of deployment do not imply any additional cost and time to enter in service provided the operator owns a licence either in the 2G/4G radio bands.

According to 3GPP standardization, both NB-IoT uplink and downlink transmissions occupy a communication bandwidth of 180 kHz in the radio portion of the electromagnetic spectrum. Moreover, as the downlink NB-IoT transmission focuses on the communication from the base station (eNB) to the user terminal (IoT device), we focus on this direction of communication to design the radio frame that should be used in the forward link of the IoT satellite system. Specifically, the downlink of NB-IoT uses few 15 kHz subcarriers, providing a sampling time unit of $T_s = 1/(15000 \times 2048)$ sec., which is identical to the one used in LTE standard. Similarly, the slot duration of NB-IoT is $T_{slot} = 15360 \times T_s = 0.5$ ms [11]. Two consecutive NB-IoT slots constitute a subframe, with at time span of 1 ms. Similarly to LTE, a group of 10 subframes with total duration $T_{frame} = 10 \times 2 \times T_s = 10$ ms is a NB-IoT frame.

Preprints (www.preprints.org) | NOT PEER-REVIEWED | Posted: 25 March 2021 doi:10.20944/preprints202103.0642.v1

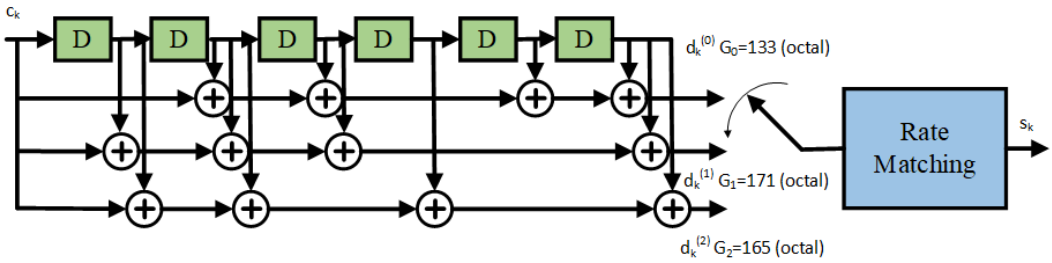

Figure 2. Overview of rate 1/3 tail biting convolutional coding with rate matching for NB-IoT [13].

The NB-IoT standard enables to repeat the transmission of the same information (block data) up to 2048 times, in order to extend the coverage range and increase the reliability of the data communication [11]. However, the higher is the number of repetitions that is performed, the lower is the spectral efficiency of the data communication that takes place. The NB-IoT link selects the Transport Block Size (TBS) on MAC layer from a variety of sizes, which range from 2 bytes (16 bits) up to 317 bytes (2536 bits) [12]. The number of Modulation and Coding Schemes (MCS) that NB-IoT supports is equal to 14, and the combination of number of subframes and MCS to be used for communication determines the code rate of the NB-IoT transmission. Regarding the error control coding, the downlink of NB-IoT uses the 1/3 tail biting convolutional encoding mother code [13]. This encoding procedure is formed by three generator polynomials, which are known as the $G_0 = 133$, $G_1 = 177$, and $G_2 = 165$ polynomials in the octal notation (see Fig. 2 for more details). Then, after channel encoding, data rate matching is utilized to obtain the desired code rate. This rate matching procedure is a puncturing process for obtaining code rates that are higher than the one provided by the mother code (*i.e.*, code rates higher than 1/3). However, in order to obtain code rates that are lower than the one provided by the mother code, the NB-IoT matching procedure combines block data repetition with puncturing [11].

The downlink of NB-IoT is formed by four channels, namely: Narrowband Physical Downlink Control Channel (NPDCCH), Narrowband Physical Downlink Shared Channel (NPDSCH), Narrowband Physical Broadcast Channel (NPBCH), and Narrowband Synchronizaton Signals (NPSS/NSSS) [14]. The first channel, the NPDCCH, is used for the control plane and provides the scheduling information for the downlink and uplink data channels. The second channel, the NPDSCH, is used for the data plane and for paging, and contains dedicated and common downlink data. The third channel, the NPBCH, contains information for the initial acquisition conveying information about the cell parameters. The NPDCCH, NPDSCH and NPBCH channels are QPSK modulated [13]. Finally, the NPSS/NSSS signals are used to cell search, time and frequency synchronization and cell identity detection, which are modulated using Zadoff-Chu sequences. In this paper, however, we will focus our attention on the QPSK modulated downlink channels.

Finally, the forward link of the satellite channel is formed by two links, namely: i) The link from the gateway to the satellite – so called feeder link, and ii) the link from the satellite to the corresponding IoT terminal - -so called access link. The satellite gateway aggregates the NB-IoT downlink channels and send them to the corresponding satellite beam. At the satellite, the received data is sent to the access beam of the corresponding IoT device. As expected, the architecture of the satellite can help to increase the throughput of the system. Toward this regard, the following section details the possible satellite architectures that can be used to transmit the data from the gateway to the NB-IoT devices.

2.2. Architectures for transmitting NB-IoT over satellite

This paper considers that in the next years the feeder links will introduce optical links to cope with the capacity demand that new 5G/6G services will require, such a the OTA applications [15]. However, the throughput of the optical links can be increased by introducing spectral efficient techniques. Specifically, this paper considers that time-packing may be one of those techniques that could enlarge their throughput. Nevertheless, the architecture of satellite's receiver is also important to increase

Preprints (www.preprints.org) | NOT PEER-REVIEWED | Posted: 25 March 2021 doi:10.20944/preprints202103.0642.v1

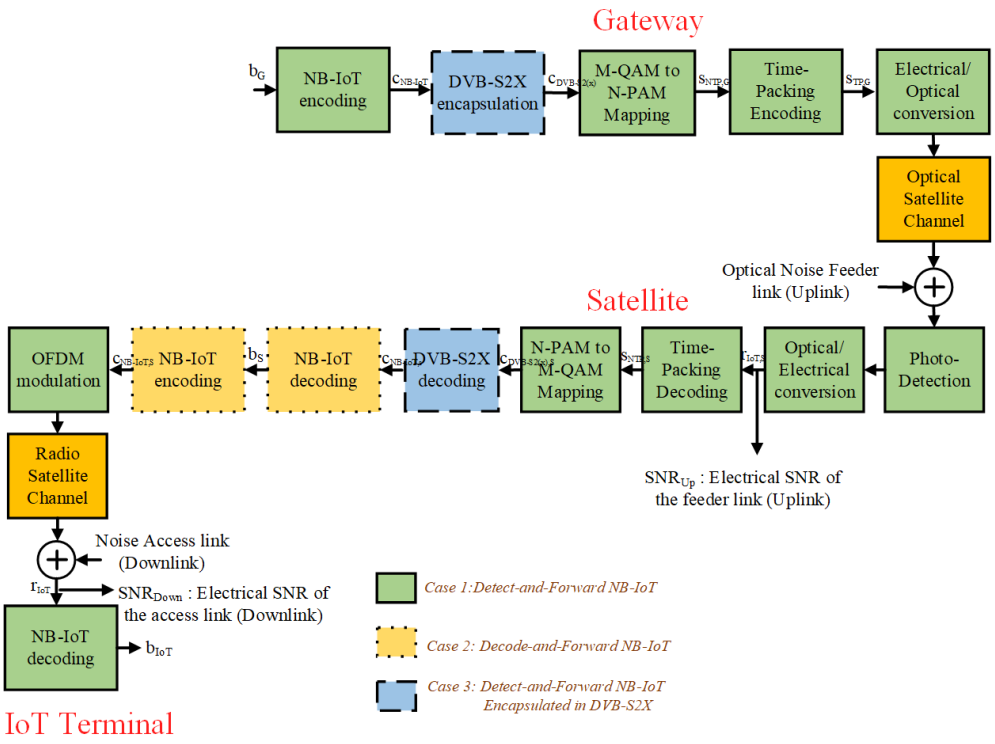

Figure 3. *Block diagram of the GEO satellite forward link for the three relaying configurations under analysis: 1) Detect-and-Forward with NB-IoT (green blocks with solid edges); 2) Decode-and-Forward with NB-IoT (orange blocks with dotted edges); and 3) Detect-and Forward with NB-IoT/DVB-S2(X) (blue blocks with dashed edges).*

the throughput of the satellite transmissions. Satellite architecture is an strategy already considered in the deployment of non-terrestrial networks by allowing bent-pipe and regenerative satellites [16]. However, this paper extends the possibilities of regenerative satellites by considering not full regeneration of the NB-IoT frames (i.e. only until the modulation stage), and the encapsulation of the NB-IoT modulated symbols in DVB-S2(X) frames. Specifically, this paper analyzes the throughput of the following satellite architectures: i) Case 1: NB-IoT modulated symbols detected at the satellite and forwarded to the corresponding IoT terminal. ii) Case 2: NB-IoT frames decoded until bit-level, re-encoded, re-mapped at the satellite and re-sent to the IoT terminal. Finally iii) Case 3: NB-IoT modulated symbols are encapsulated in DVB-S2(X) frames and re-sent to the IoT terminal (See Fig. 3).

2.2.1. *Case 1: Detect-and-Forward NB-IoT*

This strategy is similar to the transparent satellite but the optical NB-IoT modulated symbols have been time-packed. At the satellite it is removed the multi-path interference that introduces the time-packed strategy (See Section 2.3), detected the 4-PAM modulated symbols of the NB-IoT signal, remaps them to the QPSK one, OFDM modulated and re-sent to the IoT terminal. There the IoT terminal computes the LLRs of the QPSK symbols (See Section 2.4), and introduce them into the soft convolutional decoder to estimate the transmitted NB-IoT frames from the gateway (See Fig. 3).

Let $s_{NTP}[k]$ the k-th NB-IoT modulated symbols, g_{tx} the pulse-shape root rise cosine filter, T_s the Nyquist symbol time of the NB-IoT signal, and δ the time-packing overlapping factor. Then, the time-packed signal, denoted as s_{TP}, will be formulated as:

$$s_{TP}(t) = \sum_k s_{NTP}[k]\, g_{\text{tx}}\big(t - k(1-\delta)T_s\big), \tag{1}$$

Preprints (www.preprints.org) | NOT PEER-REVIEWED | Posted: 25 March 2021 doi:10.20944/preprints202103.0642.v1

Next, the Electrical-to-Optical (E/O) conversion of $s_{TP}(t)$ is given by

$$v_{\text{mzm}}(t) = V_{\text{B}} + \beta\, \widetilde{s_{TP}}(t)\, (V_\pi/\pi), \tag{2}$$

where V_{B} and V_π are the bias and half-wavelength voltages of the MZM, β is the intensity modulation index, and

$$\widetilde{s_{TP}}(t) = s_{TP}(t)/\sqrt{\mathbb{E}\{|s_{TP}(t)|^2\}} \tag{3}$$

Next, the time-packed optical signal is transmitted through the optical channel. At the satellite, it is converted from optical to electrical by the photo-detector [10], then the resulting received time-packed signal at the satellite, r_{TP}, will be equated as:

$$r_{TP}[n] = \sqrt{\left(\frac{E_b}{N_0}\right)}_{feeder} h_f \cdot s_{TP}[n] + \eta[n], \tag{4}$$

being h_f the optical channel of the feeder link (See Section 3), $s_{TP}[n]$, the n-th discrete sample of the time-packed signal, and $\eta[n]$ the resulting noise signal of unit power after the optical to electrical conversion at the satellite (See Section 4.1). The value of $(E_b/N_0)_{Feeder}$ represent the bit to noise energy ratio of the feeder link. Next the estimation of the non-time packed NB-IoT symbols at the satellite, denoted as $s_{NTP,S}$, will be obtained after equalizing the received data after match filtering the received data r_{TP} from 4 (See Section 2.3). Then, the 4-PAM modulated no-time packed signals are remapped to QPSK, OFDM modulated and transmitted to the corresponding IoT device which k-th received data, $r_{NTP,IoT}[k]$, is expressed as:

$$r_{NTP,IoT}[k] = \sqrt{\left(\frac{E_b}{N_0}\right)}_{access} \cdot h_a \cdot s_{NTP,S}[k] + \xi[k], \tag{5}$$

where $\xi[k]$ is the unit power noise signal, h_a is the acces channel, and $(E_b/N_0)_{access}$ is the bit to noise energy of the access link. Finally, the LLR of the received QPSK modulated symbols are computed, and soft-decoding it is conducted to detect the transmitted bits from the gateway, b_G (See Fig. 3).

2.2.2. *Case 2: Decode-and-Forward NB-IoT*

Similar to Case 1 (See Section 2.2.1), the satellite's receiver removes the time-packed interference (See Section 2.3), but then instead of remapping the 4-PAM modulation to QPSK, it computes the LLRs of the 4-PAM modulation that will be used by the soft-Viterbi decoder to detect the message bits transmitted from the gateway (See Section 2.4). After that, the estimated message bits are re-encoded, QPSK mapped, OFDM modulated and forwarded to the corresponding IoT device. There, the NB-IoT receiver computes the LLRs of the receive QPSK symbols to use them in the soft-Viterbi algorithm to detect the transmitted bits from the gateway.

Let $s_{NTP,S}[n]$ the estimation of the non-time packed 4-PAM modulated symbols at the satellite. Then, the following step of this case consists on computing the two LLRs per modulated symbol of the 4-PAM constellation, denoted as LLR_{b_0} and LLR_{b_1} (See Section 2.3). After that, the soft-Viterbi decoder at the satellite estimates the original transmitted bits, b_S and re-encodes them to regenerate the coded NB-IoT bits, $c_{NB-IoT,S}$, map them to QPSK symbols, $s_{NTP,S}$, and follow as in case 1 (See Fig. 3).

2.2.3. *Case 3: Detect-and-Forward NB-IoT encapsulated in DVB-S2(X)*

The third case consists on encapsulating the NB-IoT encoded bits into DVB-S2(X) frames. Next, the LDPC coded bits from DVB-S2(X) are 4-PAM modulated, pulse-shapped, time-packed and sent to the satellite. There, the time-packed interference is removed (See Section 2.3), computed the LLRs of the 4-PAM modulation and introduced in the soft-LDPC decoder of the DVB-S2(X) [17]. After that, the NB-IoT encoded bits are des-encapsulated from the DVB-S2(X) frames, mapped to QPSK,

Preprints (www.preprints.org) | NOT PEER-REVIEWED | Posted: 25 March 2021 doi:10.20944/preprints202103.0642.v1

OFDM modulated, and re-sent to the IoT device. There, it computes the LLRs of the QPSK symbols of NB-IoT frames which will be used by its soft-Viterbi decoder to detect the message transmitted from the gateway. Let $c_{NB-IoT,G}$ the NB-IoT convolutional encoded signal at the terrestrial gateway of the feeder link. Then, this signal in encapsulated in DVB-S2(X) frames. It means that the several NB-IoT convolutional words are packed to form the input message of the DVB-S2(X) physical layer frames. Recall that DVB-S(X) frames at the physical layer are in a first stage BCH encoded and in the second one LDPC encoded. The BCH encoding is used to remove the possible error floors of the LDPC decoding, which it is addressed to compensate the impairments that introduce the channel coding. In our case the optical feeder link. If $c_{DVB-S2(X),G}$ denotes the input frame to the DVB-S2(X) encoder at the gateway, it will convey P NB-IoT convolutional coded frames as: $c_{DVB-S2(X),G} = [c_{NB-IoT,G,0} \cdots c_{NB-IoT,G,P-1}]$. Next, DVB-S2(X) coded frames are 4-PAM modulated, converted from electrical to optical and sent to the satellite. There, the received optical frames and electrically converted, match filtered, and equalized to obtain the estimations of the 4-PAM symbols. Likewise case 2 are computed the two LLRs per modulated symbol, LLR_{b_0}, and LLR_{b_1} (See Section 2.3). However, they are introduced in the soft LDPC decoder instead of the soft-Viterbi decoder as it was conducted in case 2. After that, the NB-IoT encoded bits are desencapsulated from the decoded DVB-S2(X) frames, QPSK mapped, OFDM modulated and forwarded to the IoT receiver. There, at the IoT device, it is proceed as it has been explained for case 1.

2.3. Equalization of the Time-Packed signal

The three proposed transmission architectures use time-packing signalling in the optical feeder link to increase its throughput. Nevertheless, it is also introduced a self-interference that it is necessary to remove at the satellite's receiver. The optimal strategy for cancelling it consist on resorting the Maximum-Likelihood Sequence Decoding (MLSD) [18], which can be implemented in an efficient way by mean of the Viterbi Algorithm [19]. However, to increase the throughput is required to use low roll-off factors and large overlapping factors which increase the complexity of the Viterbi Algorithm notably [9]. As a result alternative strategies have to be applied. Towards this regard, it is proposed to use a two-side LMS filter to equalize the time-packed channel. Thus, the equalization strategy will consists on two steps: 1) Computing the weights of the interference canceller by means of a training sequence, and 2) Apply the pre-computed weights to the received time-packed signal from the gateway. These weights have to be computed for each overlapping factor that be used.

Let $\mathbf{r}$ the vector that stacks the samples of the time-packed signal, $\mathbf{w}$ denotes the the vector of L weighs,$\mathbf{w}$=$[w[0] \cdots w[L-1]]^T$, $\mathbf{y}$ is the buffer that contains the received samples that participates in the equalization process of the n-th time-packed received symbol, $r[n]$, $\mathbf{y}$=$[r[n-(L-1)/2] \cdots r[n] \cdots r[n+(L-1)/2]]^T$, then the equalization of the n-th transmitted symbol, denoted as $z[n]$, attains the form

$$z[n] = \mathbf{w}^T \cdot \mathbf{y} \tag{6}$$

In the training process the values of the equalized symbols, z[n], are known which permits to determine the weights. Specifically, the weights $\mathbf{w}$ have been computed by using the LMS-algorithm strategy [8,20], *i.e.*,

$$\mathbf{w}[q] = \mathbf{w}[q-1] + \mu \cdot e[q] \cdot \mathbf{y}[q] \tag{7}$$

being $\mathbf{w}[p]$ the weights of the equalizer at the p-th training iteration, μ is the forgetting parameter, and $e[p]$ is the error between the training symbol $z_t[n]$ and its estimation from (6), *i.e.* $e[n] = z_t[n] - z[n]$.

2.4. Computation of the LLRs of the 4-PAM/QPSK modulations

In this paper the NB-IoT transmitted data is encoded with a convolutional coding scheme. Furthermore, for the case 3, the encapsulated NB-IoT frames are protected using the LDPC code of DVB-S2(X) communication system. In both cases it has been used soft-decoding, and so Log-Likelihood ratios have to be determined. However IoT devices and the satellite system may be limited in their

Preprints (www.preprints.org) | NOT PEER-REVIEWED | Posted: 25 March 2021 doi:10.20944/preprints202103.0642.v1

Table 1. Closed-expressions for the LLR_{b_0} and LLR_{b_1} of the 4-PAM and QPSK modulations.

LLR_{b_m}	4-PAM	QPSK
LLR_{b_0}	$4 \cdot \mathrm{a} + log\frac{cosh(a-b)}{cosh(a+b)}$	$\frac{2 \cdot \Im(x)}{\sigma_n^2}$
LLR_{b_1}	$-2 \cdot \mathrm{b} + log\frac{cosh(c)}{cosh(a)}$	$\frac{2 \cdot \Re(x)}{\sigma_n^2}$

power consumption. Fortunately, for the 4-PAM/QPSK modulations it is possible to get reduced complexity closed-expressions for achieving optimal LLR computation. The 4-PAM modulation is used in the feeder link of the satellite whereas the QPSK modulation is used in the access link. Both use Gray-mapping and their corresponding modulation symbols are : $\mathbf{s_{4-PAM}} = \{-3,-1,1,3\}/\sqrt{5}$, and $\mathbf{s_{QPSK}} = \{-1-j, 1-j, 1+j, -1+j\}/\sqrt{2}$ (see Fig. 4). Given that theses modulations transport two bits per modulated symbol it will be necessary to compute two LLRs per modulated symbol. Thus the expression for computing the LLRs becomes

$$LLR_{b_m} = -log\frac{\left(\sum_{\substack{p=0 \\ s_p|b_m=0}}^{M/2} e^{-\frac{|z-h\cdot s_p|^2}{2\sigma_n^2}}\right)}{\left(\sum_{\substack{q=0 \\ s_q|b_m=1}}^{M/2} e^{-\frac{|z-h\cdot sq|^2}{(2\sigma_n^2}}\right)}, \tag{8}$$

being LLR_{b_m} the LLR of the m-th bit of the modulated symbol, σ_n^2 is the noise power, M is the number of constellation symbols, h is the communication channel, z is the received data at the input of the demapping, s_p and s_q symbolize the constellation symbols which m-th bit is 0, and 1 respectively. Thus according to (8) and the gray mapping proposed in Fig. 8, the LLR of the first bit, b_0, denoted as LLR_{b_0}, for the 4-PAM and QPSK modulations will be computed as

$$LLR_{b_0} = -log\frac{\left(e^{-\frac{|z-h\cdot s_0|^2}{2\sigma_n^2}} + e^{-\frac{|z-h\cdot s_1|^2}{2\sigma_n^2}}\right)}{\left(e^{-\frac{|z-h\cdot s_2|^2}{2\sigma_n^2}} + e^{-\frac{|z-h\cdot s_3|^2}{2\sigma_n^2}}\right)}, \tag{9}$$

whereas LLR of the second bit, b_1, symbolized as, LLR_{b_1}, for the 4-PAM and QPSK modulations will be determined as:

$$LLR_{b_0} = -log\frac{\left(e^{-\frac{|z-h\cdot s_0|^2}{2\sigma_n^2}} + e^{-\frac{|z-h\cdot s_3|^2}{2\sigma_n^2}}\right)}{\left(e^{-\frac{|z-h\cdot s_1|^2}{2\sigma_n^2}} + e^{-\frac{|z-h\cdot s_2|^2}{2\sigma_n^2}}\right)}. \tag{10}$$

If (9) and (10) are developed for the 4-PAM and QPSK modulation symbols, we obtain the following expressions for LLR_{b_0} and LLR_{b_1} (See Table 1).There the constants for computing the LLR_{b_0} and LLR_{b_1} of the 4-PAM modulation are equal to: $a = 2 \cdot z \cdot s_1/(2 \cdot \sigma_n^2)$, $b = 4 \cdot s_1^2/(2\sigma_n^2)$, and $c = 3 \cdot a$, being s_1 the second symbol of the 4-PAM constellation, i.e. $s_1 = -1/\sqrt{5}$ (See Fig. 4). The signal z represents the data after equalizing the time-packed signal (See Section 2.3). For case 2 this signal corresponds to the NB-IoT one, and its LLRs will be introduced in the soft-convolutional decoder for recovering the transmitted message to regenerate the NB-IoT signal. For case 3, the signal z corresponds to the DVB-S2(X) after the time-packing equalization. The computed LLRs for this case will be introduced to the LDPC decoder of DVB-S2(X) [17]. After that, the encoded NB-IoT bits are QPSK mapped, OFDM modulated and forwarded to the IoT-device. Finally, at the IoT's receiver the LLRs of the received QPSK modulation symbols are computed for all cases under study. These LLRs will be used by the soft-Viterbi decoder to recover the message transmitted from the ground station.

Preprints (www.preprints.org) | NOT PEER-REVIEWED | Posted: 25 March 2021 doi:10.20944/preprints202103.0642.v1

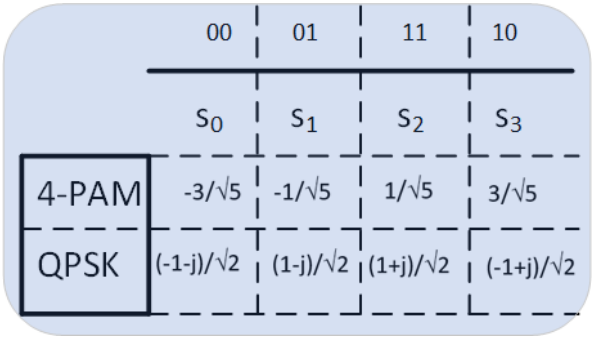

Figure 4. *Mapping between 4-PAM and QPSK/4-PAM symbols and the binary gray mapping.*

3. Optical Wireless Satellite Channel Model

The optical signal that is used to transport the data symbols from the ground station to the GEO satellite must go through the different layers of the Earth's atmosphere. Unfortunately, the power loss that the optical feeder link experiences in the *uplink* direction of communication is larger than the one observed in *downlink*. This is because, in the ground-to-satellite communication, the optical signal starts to spread and accumulate distortion as soon as it leaves the ground station transmitter.

3.1. Atmospheric power losses: Absorption and scattering modelling

The power loss of the optical feeder link is a function of the atmospheric attenuation, which depends on both absorption and scattering effects that the light signal experiences while propagating [21]. To compute this value, the atmospheric attenuation coefficient

$$\gamma_{\text{atm}} = \alpha_{\text{m}} + \alpha_{\text{a}} + \beta_{\text{m}} + \beta_{\text{a}} \tag{11}$$

needs to be computed, where α_{m} and α_{a} are the molecular and aerosol absorption coefficients, respectively, whereas β_{m} and β_{a} are the molecular and aerosol scattering coefficients, respectively.

Modelling of absorption: At Infrared (IR) wavelengths, the principal atmospheric absorbers are the molecules of water, carbon-dioxide, and ozone. As expected, the atmospheric absorption is a wavelength-dependent phenomenon. Therefore, the operating wavelength for optical feeder link transmissions should be chosen to minimize this loss, using the atmospheric transmission windows in which the molecular and aerosol absorption is less than 0.2 dB/km for clear sky conditions [22]. In addition to the low-absorption requirements, most optical feeder links are designed to work in the 780-850 nm and 1520-1600 nm windows because there are lasers and detectors commercial available to work in these wavelengths.

Modelling of scattering: Like absorption, scattering is also a phenomenon that is strongly dependent on the operating wavelength. If the size of the atmospheric particles is small in comparison to the optical feeder link wavelength, then *Rayleigh scattering* is produced. Particles like air molecules and haze cause Rayleigh scattering [23] and affect notably optical wireless transmissions in the Visible Light (VL) and Ultraviolet (UV) regions; on the other hand, Rayleigh scattering can be neglected for optical feeder link wavelengths in the IR range (*i.e.*, when $\lambda \gg 1\,\mu$m). Similarly, when the atmospheric particles size is comparable with the operating wavelength, then *Mie scattering* is produced. Aerosol particles, fog and haze are the major contributors of Mie scattering, and this phenomenon is dominant for wavelengths in the IR range. Finally, if the atmospheric particles are much larger than the operating wavelength, the scattering is better described by geometrical optical models, which should be used in case of rain, snow and hail weather conditions [24].

Modelling of the atmosphere's transmittance: Apart from the previously described λ-dependent effects, the specific value that the atmospheric attenuation coefficient takes depends on the

Preprints (www.preprints.org) | NOT PEER-REVIEWED | Posted: 25 March 2021 doi:10.20944/preprints202103.0642.v1

concentration of molecules (and aerosols) of the Earth's atmosphere at different altitudes h. Based on this assumption, the atmospheric transmittance that an optical feeder link with zenith angle ζ experiences is given by

$$T_{\text{atm}}(\lambda) = \exp\left\{ -\sec(\zeta) \int_{h_0}^{H} \gamma(\lambda, h)\, dh \right\}, \tag{12}$$

where h_0 is the altitude of the ground station over the sea level, H is the vertical height at which the GEO satellite is placed, and $\gamma(\lambda, h)$ is the attenuation coefficient at wavelength λ and altitude h. Based on this formula, it is possible to see that atmospheric transmittance is increased at low zenith angles (*i.e.*, at high elevation angles), as the fraction of the incident electromagnetic power that is transferred through the atmosphere layers is increased.

Power losses due to fog: From the common weather conditions, fog is the one that contributes most in the absorption and scattering of the optical signal when propagates through the Earth's atmosphere. In presence of fog, the optical feeder link connectivity is put at risk seriously, particularly when the fog layer next to the ground station extends vertically very high, forming a fog layer that can be as thick as 400 m over the Earth's surface. In such critical weather conditions, the use of very high power lasers (1550 nm) with special mitigation techniques is the only option to maximize the chances of optical feeder link connectivity. As an alternative method to the Mie scattering theory, the attenuation due to fog for different wavelengths can be estimated using empirical models that use as input parameter the visibility in km measured on the VL region (550 nm). For a comparison of the fog attenuation at different wavelengths (850 nm and 950 mn), please refer to [25]. Note that in extreme cases, where the visibility due to fog is reduced to about 50 m, atmospheric attenuation can be as high as 350 dB/km [26].

Power losses due to rain: The impact of rain in the propagation of optical signals is not as pronounced as fog, because the size of the rain droplets are significantly larger in size (from 100 μm to 1000 μm) when compared to operating wavelengths of optical feeder links. For example, the attenuation loss in light rain (2.5 mm/h) to heavy rain (25 mm/h) ranges from 1 dB/km to 10 dB/km for 850 nm and 1550 nm operating wavelengths [27]. It is important to note that the low clouds that are usually accompanying the rainy weather are the source of strong attenuation in most optical feeder link transmissions. In order to combat the huge power loss that takes place in such conditions, it is recommended to include a few tens-of-dB margin (*e.g.*, 30 dB) when dimensioning the link budget of the optical wireless link. Moreover, optical feeder link designers can also implement adaptive coding and modulation schemes to address the varying weather conditions in the geographical area around the ground station [8].

Power losses due to snow: Finally, since the size of snow droplets is between the size of rain and fog droplets, the atmospheric attenuation for dry/wet snow conditions is usually stronger than the one in presence of rain, but not as severe as the one in case of fog. However, during heavy snow storms, the path of the optical feeder link can be completely blocked for the presence of densely-packed snow flakes in the propagation path. In such cases, the attenuation is similar to the one observed in foggy weather (30-350 dB/km) and, as expected, can seriously put at risk the optical feeder link connectivity.

3.2. Atmospheric turbulence: Beam wander, Beam spreading, and Beam scintillation

Atmospheric turbulence is a random phenomenon that is caused by the variation of the temperature and pressure on the atmosphere layers that are in the propagation path of the optical wireless signal. These temperature and pressure inhomogeneities form turbulent cells, known as *eddies*, which have different sizes and different diffractive indexes. The eddies act as if prisms/lenses were deployed in the propagation path, introducing constructive and destructive interference in the received optical signal. The perturbations that atmospheric turbulence introduces in the wavefront of the optical beam can be physically described by the Kolmogorov model [28]. Depending on the size of the turbulent eddies with respect to the transmitted beam size, thee types of atmospheric turbulence-induced effects can be identified, namely: *Beam wander*, *beam spreading*, and *beam scintillation*.

Preprints (www.preprints.org) | NOT PEER-REVIEWED | Posted: 25 March 2021 doi:10.20944/preprints202103.0642.v1

Turbulence-induced beam wander: This phenomenon takes place when the size of the turbulent eddies is *larger* than the size of the optical beam. Beam wander results in a random deviation of the optical beam from its planned (rectilinear) propagating path and, in extreme displacement situations, may lead to the failure of the optical wireless link. Beam wander is a major concern in the uplink transmission of an optical feeder link, as the beam size in the ground-to-satellite transmission is often smaller than the size of the turbulent eddies, resulting in a beam displacement at the receiver side that can be as large as several hundreed meters.

In case of a collimated beam (plane wave model), the Root Mean Square (RMS) displacement due to beam wander for an uplink path with zenith angle ζ can be written as

$$\sigma_{\mathrm{BW}}^2 = 7.25\,(H-h_0)^2\sec^3(\zeta)\,{W_0}^{-1/3}\int_{h_0}^{H} C_n^2(h)\left(1-\frac{h-h_0}{H-h_0}\right)^2 dh \tag{13}$$

$$\cong 0.54(H-h_0)^2\sec^2(\zeta)\left(\frac{\lambda}{2W_0}\right)^2\left(\frac{2W_0}{r_0}\right)^{5/3}, \tag{14}$$

where H is the altitude of the GEO satellite (receiver), h_0 is the altitude of ground station (transmitter), W_0 is the initial beam size, and r_0 is the atmospheric coherence width, which is also known now as *Fried's coherence length*, *Fried's parameter*, or simply coherence length [29]. The Fried's coherence length is a widely used descriptor of the level of atmospheric turbulence at a particular site and, for a known structure constant profile $C_n^2(h)$ and plane wave model (collimated beam), it is given by [30]

$$r_0 = \left[0.423\,k^2\sec(\zeta)\int_{h_0}^{H} C_n^2(h)\,dh\right]^{-3/5}, \tag{15}$$

where $k = 2\pi/\lambda$ is the wavenumber of the optical beam. As expected, $C_n^2(h)$ varies with the time of the day, the geographical location, and the altitude. Therefore, for vertical optical links (slant paths), the value of $C_n^2(h)$ has to be integrated over the complete propagation path, starting from the height of the ground station above the sea level and ending at the altitude in which the Earth's atmosphere vanishes (*i.e.*, at about 40 km).

Various empirical models for $C_n^2(h)$ have been proposed in the literature to estimate the turbulence profiles, using as reference the experimental measurements that were carried out at different geographical locations, time of the day, wind speed, terrain types, among others. The most widely used model to characterize the refractive index structure of the atmosphere for vertical links (slant paths) is the so-called Hufnagel-Valley (H-V) model [29], *i.e.*,

$$C_n^2(h) = A_0\exp\left(-\frac{h}{100}\right) + 5.94\times10^{-53}\left(\frac{v}{27}\right)^2 h^{10}\exp\left(-\frac{h}{1000}\right) + 2.7\times10^{-16}\exp\left(-\frac{h}{1500}\right), \tag{16}$$

where h [m] is the altitude, v [m/s] is the Root-Mean-Square (RMS) wind-speed, and parameter $A_0 = C_n^2(h_0)$ [$\mathrm{m}^{-2/3}$] is the nominal value of the refractive index near the ground level. The RMS wind-speed in (16) is determined from the Bufton wind model, and can take values that range from $v = 10$ to 30 m/s for moderate and strong wind speeds, respectively. Similarly, the ground turbulence level can take values between $A_0 = 1.7\times10^{-14}$ and $1.7\times10^{-13}\,\mathrm{m}^{-2/3}$, which depends on the location and day time, among other parameters.

When using $A_0 = 1.7\times10^{-14}\,\mathrm{m}^{-2/3}$ and $v = 21$ m/s, this modeled is commonly referred as the *H-V*$_{5/7}$ *model* because, for wavelength $\lambda = 0.5$ μm and a transmitter on the ground looking up (*i.e.*,

Preprints (www.preprints.org) | NOT PEER-REVIEWED | Posted: 25 March 2021 doi:10.20944/preprints202103.0642.v1

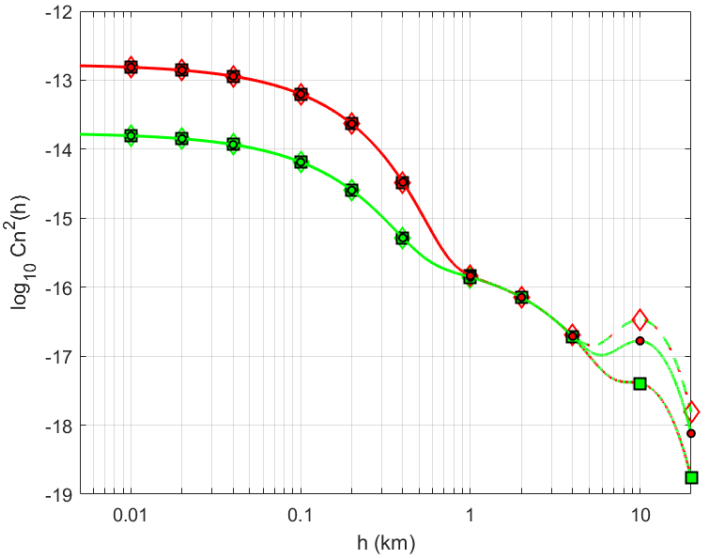

Figure 5. *Refractive index structure $C_n^2(h)$ along the slant path for the H-V day model as function of the altitude. Red lines: $A_0 = 1.7 \times 10^{-13}\ m^{-2/3}$. Green lines: $A_0 = 1.7 \times 10^{-14}\ m^{-2/3}$. Wind speed: $v = 10$ m/s (dotted lines with squares); $v = 21$ m/s (solid-lines with circles); $v = 30$ m/s (dashed lines with diamonds).*

with $\zeta = 0$ deg.), it predicts a value of atmospheric coherence diameter $r_0 = 5$ cm according to (15) and a value of isoplanatic angle

$$\theta_0 = \frac{\cos^{8/5}(\zeta)}{\left[2.91\, k^2 \int_{h_0}^{H} C_n^2(h)\, (h - h_0)^{5/3}\, dh\right]^{3/5}} \tag{17}$$

of 7 μrad in case of a spherical wave with output-plane beam parameters $\Theta = \Lambda = 0$. The refractive index profile along the vertical/slant path is shown in Fig. 5 for two nominal values of refractive index at the ground level and three different RMS wind speeds. From this figure, it is possible to observe that the ground turbulence level A_0 has little effect above 1 km, and that the wind speed governs the profile behavior primarily in the vicinity of altitudes in the 10 km range.

Similarly, Fig. 6 shows the RMS angular displacement due to beam wander (σ_{BW}^2) as function of the beam radius W_0, when the operating wavelength $\lambda = 1.55\mu$m and the refractive index structure $C_n^2(h)$ follows the H-V$_{5/7}$ model. As expected, the RMS beam wander displacement is higher for the largest zenith angle, as the section of the atmosphere through which the optical beam needs pass through is thicker, the beam deviation with respect to the straight path grows. Finally, according to (15), the Fried's coherence length $r_0 = 19.25$ and 12.70 cm for zenith angle $\zeta = 0$ and 60 deg., respectively.

Turbulence-induced beam spreading: This phenomenon takes place when the turbulent eddies are *smaller* than the size of the optical beam. Beam spreading generates a widening of the beam size, beyond the natural broadening due to diffraction that the non-turbulent atmosphere introduces. Beam spreading does not affect the direction of the optical beam but, in contrast, reduces the optical power at the receiver aperture due to the energy dispersion that takes place.

Turbulence-induced beam scintillation: When the size of turbulent eddies is of the *same order* of the size of the optical beam, then the eddies act as lenses that focus and defocus the incoming beam. In this situation, the eddies lead to a redistribution of the signal energy that generates a temporal and spatial fluctuation of the irradiance at the receiver aperture. This phenomenon, which is known as *scintillation*, represent one of the major sources of degradation in the performance of an optical feeder

Preprints (www.preprints.org) | NOT PEER-REVIEWED | Posted: 25 March 2021 doi:10.20944/preprints202103.0642.v1

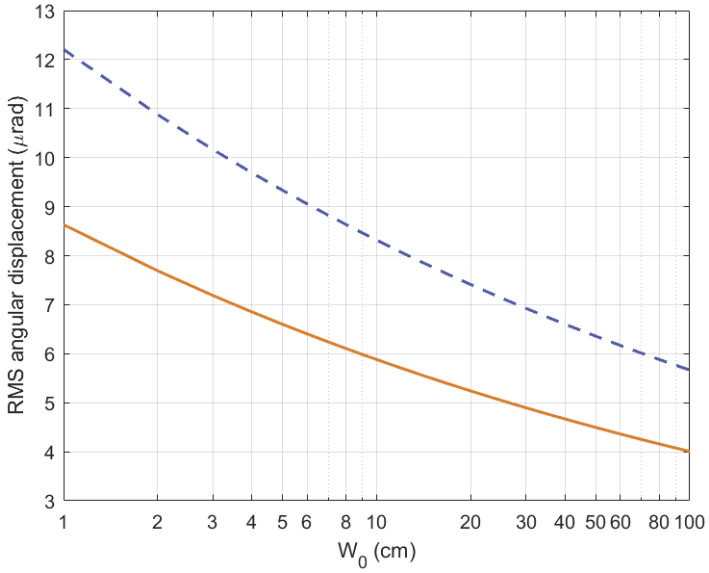

Figure 6. *RMS angular beam wander (σ^2_{BW}) as function of the beam radius (W_0) for a transmitter in the ground and a satellite in the space assuming $\lambda = 1.55$ μm and a refractive index structure following the H-$V_{5/7}$ model (wind speed: $v = 21$ m/s). Zenith angle: $\zeta = 0$ deg. (solid orange line) and $\zeta = 60$ deg. (dashed purple line).*

link. Atmospheric turbulence also leads to loss of spatial coherence of an initially coherent optical beam, and may also produce depolarization of the light and temporal stretching of the optical pulse.

The atmospheric scintillation is measured in terms of the scintillation index, which is the normalized variance of the intensity fluctuations, *i.e.*,

$$\sigma_I^2 \triangleq \frac{\langle (I - I_m)^2 \rangle}{I_m^2} = \frac{\langle I^2 \rangle - I_m^2}{I_m^2} = \frac{\langle I^2 \rangle}{I_m^2} - 1, \qquad I_m = \langle I \rangle, \tag{18}$$

where I is the irradiance (intensity) in the detector plane and $\langle \cdot \rangle$ denotes the ensemble average.

The Gamma-Gamma distribution has been proposed to describe the turbulence-induce scintillation over a broad range of beam diameters. The Probability Density Function (PDF) of the Gamma-Gamma turbulence model and the scintillation index are given by

$$f_I(x) = \frac{2}{\Gamma(\alpha)\Gamma(\beta)x}\left(\frac{\alpha\beta x}{I_m}\right)^{\frac{\alpha+\beta}{2}} K_{\alpha-\beta}\left(2\sqrt{\frac{\alpha\beta x}{I_m}}\right) \qquad x \geq 0, \qquad \sigma_I^2 = \frac{1}{\alpha} + \frac{1}{\beta} + \frac{1}{\alpha\beta}, \tag{19}$$

respectively, where I_m denotes the mean irradiance, $\Gamma(x)$ is the Gamma function, $K_n(x)$ is the modified Bessel function of the second kind. The parameters $\alpha = 1/\sigma_{\mathrm{X}}^2$ and $\beta = 1/\sigma_{\mathrm{Y}}^2$ of the Gamma-Gamma distribution in (19) are directly related to the atmospheric conditions, and for the untracked beam case are given

$$\sigma_{\mathrm{X}}^2 = 5.95(H - h_0)^2 \sec^2(\zeta)\left(\frac{2W_0}{r_0}\right)^{5/3}\left(\frac{\alpha_{\mathrm{pe}}}{W}\right)^2 \exp\left\{\frac{0.49\,\sigma_{\mathrm{Bu}}^2}{\left[1 + (1+\Theta)\,0.56\,\sigma_{\mathrm{Bu}}^{12/5}\right]^{7/6}}\right\} - 1, \tag{20}$$

and

$$\sigma_{\mathrm{Y}}^2 = \exp\left\{\frac{0.51\,\sigma_{\mathrm{Bu}}^2}{\left[1 + 0.69\,\sigma_{\mathrm{Bu}}^{12/5}\right]^{5/6}}\right\} - 1. \tag{21}$$

Preprints (www.preprints.org) | NOT PEER-REVIEWED | Posted: 25 March 2021 doi:10.20944/preprints202103.0642.v1

The various parameters that appear in equations (20) and (21) are defined as follows:

$$\alpha_{\text{pe}} = \sigma_{\text{pe}}/L, \qquad \sigma_{\text{pe}}^2 \cong \sigma_{\text{BW}}^2\left[1-\left(\frac{C_r^2W_0^2/r_0^2}{1+C_r^2W_0^2/r_0^2}\right)^{1/6}\right], \qquad L=\frac{H-h_0}{cos(\zeta)}, \qquad C_r = 2\pi, \tag{22}$$

are the jitter-induced angular pointing error, the pointing error variance, slant path length, and scaling constant, respectively. Similarly, the diffractive beam radius at the receiver is given by

$$W = W_0\sqrt{\Theta_0^2+\Lambda_0^2}, \qquad \text{where} \qquad \Theta_0 = 1-\frac{L}{F_0}, \qquad \Lambda_0 = \frac{2L}{kW_0^2} \tag{23}$$

are the *input-plane beam parameters*. Note that for a collimated beam, the phase front radius of curvature at the transmitter output aperture $F_0 \to \infty$ and, due to that, $\Theta_0 \cong 1$. Finally, the irradiance flux variance in the focal plane of the receiver

$$\sigma_{\text{Bu}}^2 = 8.7\,k^{7/6}(H-h_0)^{5/6}\text{sec}^{11/6}(\zeta)\times \text{Re}\left\{\int_{h_0}^{H} C_n^2(h)\left[\xi^{5/6}\left[\Lambda\xi+\text{j}(1-\overline{\Theta}\xi)\right]^{5/6}-\Lambda^{5/6}\xi^{5/3}\right]dh\right\}, \tag{24}$$

where

$$\xi = 1-\frac{h-h_0}{H-h_0} \tag{25}$$

is the normalized distance for the uplink propagation path, and

$$\overline{\Theta} = 1-\Theta = 1-\frac{\Theta_0}{\Theta_0^2+\Lambda_0^2} = -\frac{L}{F_0}, \qquad \Lambda = \frac{\Lambda_0}{\Theta_0^2+\Lambda_0^2} = \frac{2L}{kW^2}, \tag{26}$$

are the *output-plane beam parameters*.

In Fig. 7 we plot the corresponding Gamma-Gamma PDF for three different beam sizes W_0, which are equal to 1, 10 and 50 cm. Once again, the wavelength was set to $\lambda = 1.55\,\mu$m and the analysis was done for the uplink direction of communication of a perfectly vertical GEO satellite feeder link (*i.e.*, $\zeta = 0$ deg. and $H = 36000$ km) when using the H-V$_{5/7}$ refractive index model (*i.e.*, $v = 21$ m/s). Note that in this situation, the Fried's coherence length is $r_0 = 19.25$ cm. As expected, for small beam sizes in which the $2W_0/r_0 \ll 1$ relationship is verified (*e.g.*, similar to $W_0 = 1$ cm in Fig. 7) the longitudinal component of the scintillation index will be much less than 1; due to that, the corresponding PDF of the normalized irradiance will have a shape that resembles the one of a log-normal distribution, but with some differences in the upper and lower tails. On the other hand, for large beams in which the $2W_0/r_0 \gg 1$ relationship is observed (*e.g.*, similar to $W_0 = 50$ cm in Fig. 7), the scintillation index becomes larger than 1 and the shape of the PDF starts to resemble a negative exponential distribution.

4. Performance Evaluation

The error correction capabilities that the Modulation and Coding Schemes (MCS) of the NB-IoT (and DVB-S2(X)) standard have on the end-to-end forward link of the GEO satellite system (*i.e.*, from the satellite gateway to the IoT terminals) is now evaluated in detail. For this purpose, we first present the simulation setup and, after that, we show the different figures of merit that are relevant to characterize the end-to-end performance of the three GEO satellite relaying configurations.

4.1. Simulation setup of the Optical channel

According to the analysis presented in [10], the mean SNR of the electrical signal that is direct-detected by the PD that is placed on-board the satellite is given by

$$\text{SNR}_{\text{e,pd}} = \frac{\mathbb{E}\{|i_{\text{d}}(t)|^2\}}{\mathbb{E}\{|n_{\text{o}}(t)|^2\}} \approx \frac{I_D^2\,\beta^2}{\mathbb{E}\{|n_{\text{o}}(t)|^2\}} \qquad \beta \ll 1, \tag{27}$$

Preprints (www.preprints.org) | NOT PEER-REVIEWED | Posted: 25 March 2021 doi:10.20944/preprints202103.0642.v1

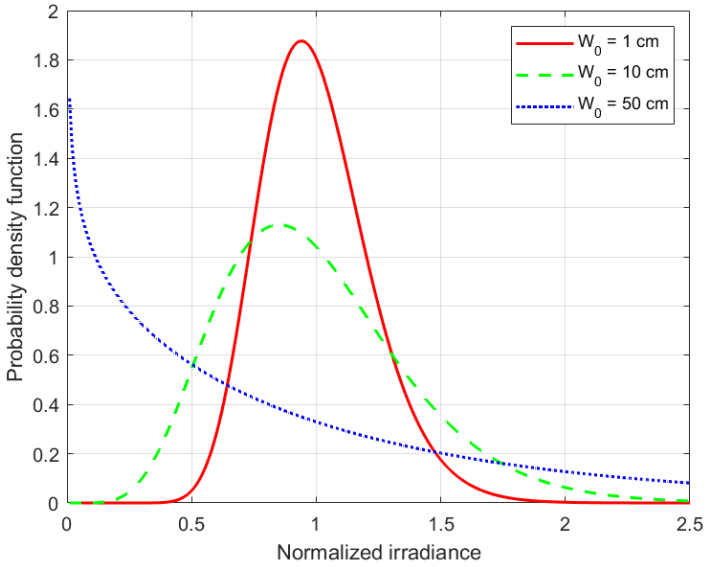

Figure 7. *Gamma-Gamma probability density function for an untracked collimated beam plotted as function of the normalized irradiance for a GEO optical feeder uplink channel with zenith angle $\zeta = 0$ deg. and H-$V_{5/7}$ refractive index structure ($\lambda = 1.55\,\mu m$, $r_0 = 19\,cm$). Beam radius: $W_0 = 1\,cm$ (solid red lines), $W_0 = 10\,cm$ (dashed green lines), and $W_0 = 50\,cm$ (dotted blue lines).*

where

$$I_{\mathrm{D}} = \mathbb{E}\{i_{\mathrm{D}}(t)\} = \mu \, \frac{G_{\mathrm{o,tx}}\, G_{\mathrm{o,rx}}\, G_{\mathrm{o,edfa}}}{L_{\mathrm{o,fsl}}\, L_{\mathrm{o,atm}}\, L_{\mathrm{o,bsl}}\, L_{\mathrm{o,sys}}} \, \frac{P_{\mathrm{o,ld}}}{2} \tag{28}$$

is the DC component of the time-varying electrical current $i_{\mathrm{D}}(t)$ that the PD generates when being excited by the intensity modulated optical signal, β is the intensity modulation index, and

$$\mathbb{E}\{|n_{\mathrm{o}}(t)|^2\} = \mathbb{E}\{|i_{\mathrm{shot}}(t)|^2\} + \mathbb{E}\{|i_{\mathrm{thermal}}(t)|^2\} + \mathbb{E}\{|i_{\mathrm{rin}}(t)|^2\} + \mathbb{E}\{|i_{\mathrm{beat}}(t)|^2\} \tag{29}$$

includes the contribution of all noise sources in the optical feeder link, namely the *shot noise* sources, *thermal noise*, *Relative Intensity Noise* (RIN) of LD, and *beat noise* [7]. Note that shot noise term includes the contribution of the received optical signal, the Amplified Spontaneous Emission (ASE) noise, the background optical noise and the dark current noise, whereas the beat noise term accounts the effect of combining the received optical signal with the ASE noise.

When the received optical power is between -90 and -20 dBW, it can be shown that the beat noise between received optical signal and ASE noise dominates the SNR performance of the optical feeder link [31]. In this situation,

$$\mathbb{E}\{|n_{\mathrm{o}}(t)|^2\} \approx \mathbb{E}\{|i_{\mathrm{beat}}(t)|^2\} = i^2_{\mathrm{sig-sp}} + i^2_{\mathrm{sp-sp}} \approx i^2_{\mathrm{sig-sp}} = 4\, I_{\mathrm{D}}\, I_{\mathrm{ase}} \left(B_{\mathrm{e}} / B_{\mathrm{o}}\right), \tag{30}$$

where B_{o} is the bandwidth of the optical signal at the PD input, B_{e} is the bandwidth of the electrical signal at the PD output, and $I_{\mathrm{ase}} = \mu\, G_{\mathrm{o,edfa}}\, P_{\mathrm{ase}}$ is the DC component generated by the ASE noise, whose equivalent noise power at the input of the EDFA is given by $P_{\mathrm{ase}} = \rho_{\mathrm{ase}}\, B_{\mathrm{o}}$.

Table 2 summarizes the parameters of the optical feeder link, taking into account both the optical gains and losses, as well as the different sources of optical noise [7,32]. The effect of any other parameter not listed in this table is considered negligible. When $L_{\mathrm{o,atm}} = 0$ dB (*i.e.*, clear-sky conditions), the DC current at the PD output is $I_{\mathrm{D}} = 75.68$ mA, whereas the DC current generated by the ASE noise is $I_{\mathrm{ase}} = 0.125$ mA regardless of the weather. Thus, when we set the intensity modulation index $\beta = 0.5$, the SNR of the electrical signal at the PD output becomes

$$\mathrm{SNR}_{\mathrm{e,pd}}[\mathrm{dB}] = 25.01[\mathrm{dB}] - L_{\mathrm{o,atm}}[\mathrm{dB}]. \tag{31}$$

Preprints (www.preprints.org) | NOT PEER-REVIEWED | Posted: 25 March 2021 doi:10.20944/preprints202103.0642.v1

Table 2. *Parameters of the optical feeder link used in the NB-IoT satellite system and associated power budget.*

Symbol	Optical Link Parameter	Value	Unit
$P_{o,ld}$	Optical power of LD (including EDFA booster)	47.0	dBm
$G_{o,tx}$	Optical gain of transmitter (ground telescope)	110.9	dBi
$G_{o,rx}$	Optical gain of receiver (satellite telescope)	112.8	dBi
$L_{o,fsl}$	Free space loss of optical link ($\lambda = 1550$ nm, $H = 36000$ km)	289.8	dB
$L_{o,atm}$	Atmospheric attenuation (absorption and scattering)	0-10	dB
$L_{o,bsl}$	Beam spreading loss due to scintillation	1.6	dB
$L_{o,sys}$	System losses in the optical feeder link	4.5	dB
G_{edfa}	Gain of the optical amplifier (EDFA)	50.0	dB
μ	Responsivity of photodetector (PIN diode)	0.5	A/W
B_e	Bandwidth of electrical filter (PD output)	1.5	GHz
B_o	Bandwidth of optical channel ($\lambda = 1550$ nm)	12.5	GHz
ρ_{ase}	PSD of amplified spontaneous emissions	2.0×10^{-19}	W/Hz
ρ_{rin}	PSD of RIN process (normalized)	-160	dBc/Hz
ρ_{back}	PSD of background noise at EDFA input	7.6×10^{-25}	W/Hz
i_n	Electrical noise current spectral density	1.0×10^{-11}	A
i_{dark}	Dark current at the PIN diode output	1.0×10^{-10}	A

Note that for larger intensity modulation indexes β, the non-linear distortion introduced by the Match-Zehnder Modulator (MZM) of the optical transmitter becomes more notable. For those situation, the use of Digital Pre-Distortion (DPD) is needed to keep non-linear distortion under control [7].

Fig. 8 shows the Cumulative Distribution Function (CDF) of the power loss that turbulence-induced beam wander and beam scintillation introduce on the received optical power of the optical uplink transmission in the satellite forward link. Without loss of generalization, it is assumed that the ground station is placed next to the city of Madrid, Spain (*i.e.*, Lat. 40.43^o North, Long. 4.25^o West, and altitude $h_0 = 864$ m), with an expected system availability due to cloud-free line-of-sight conditions close to 99.8%. Similarly, the satellite is assumed to be placed in the GEO positon of 19.2^o East at an altitude of $H = 36000$ km, giving as result a zenith angle $\zeta = 52.61$ deg. for the optical feeder link in the uplink direction of communication. The nominal value of the refractive index near the ground level is always $A_0 = 1.7 \times 10^{-14}\,\mathrm{m}^{-2/3}$, and the CDF is plotted for three different wind speeds (*i.e.*, $v = 10, 21$ and 30 m/s). Note that when $v = 21$ m/s, the refractive index model becomes the well-known H-V$_{5/7}$ model. Finally, an untracked collimated beam is assumed, with a beam radius of $W_0 = 10$ cm at a wavelength of $\lambda = 1550$ nm. As expected, the stronger is the wind speed, the more variability is introduced in the instantaneous intensity of the received optical signal at the GEO satellite. For example, the 10-th percentile for the turbulence-induced power loss (*i.e.*, power loss margin for a 90% link availability without coding) is equal to 2.4, 3.0 and 3.8 dB for a wind speed of 10, 21 and 30 m/s, respectively. These turbulence-induced power losses grow to 4.3, 5.4 and 7.0 dB when we study the 1-st percentile (*i.e.*, power loss margin for a 99% link availability without coding) the for the same three values of wind speeds (*i.e.*, 10, 21 and 30 m/s, respectively).

4.2. Simulation setup of NB-IoT signal

This paper evaluates the BLER and Throughput of the following three forward link architectures for transmitting NB-IoT over satellite when the feeder link is optical:

1. *Case 1: NB-IoT detect-and-forward (See Section 2.2.1).*
2. *Case 2: NB-IoT decode-and-forward (See Section 2.2.2).*
3. *Case 3: NB-IoT encapsulated in DVB-S2(X) frames. DVB-S2(X) decode and NB-IoT detect-and- forward (See Section 2.2.3).*

In all cases the frame length of the NB-IoT has been kept constant to N=1032 bits. The pulse-shape for NB-IoT and DVB-S2(X) waveforms is the square-root rise cosine filter (RRC) with a roll-off factor of ρ=0.15. The tested time-packed overlapping factor, denoted as δ, takes the following values

Preprints (www.preprints.org) | NOT PEER-REVIEWED | Posted: 25 March 2021 doi:10.20944/preprints202103.0642.v1

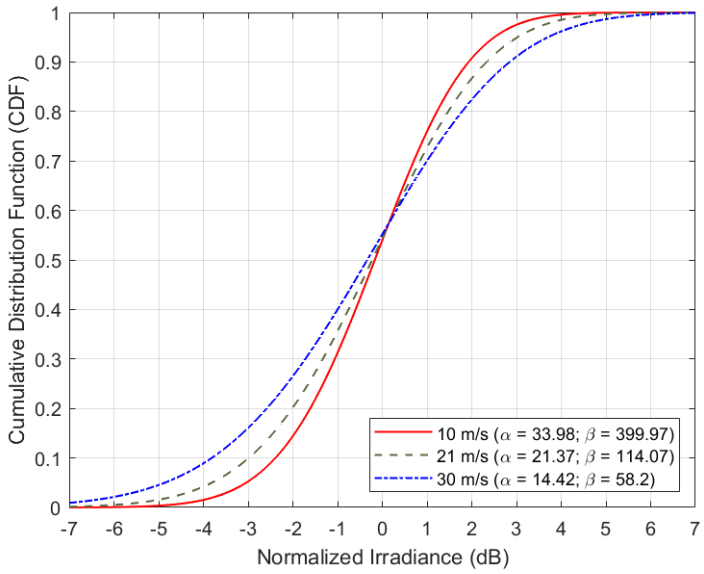

Figure 8. *Cumulative distribution function of the power loss that turbulence-induced beam wander and scintillation introduces in the uplink direction of the optical feeder link in case of an untracked collimated beam with $\lambda = 1.55\,\mu m$, $W_0 = 10\,cm$, $\zeta = 52.61\,deg$, $A_0 = 1.7 \times 10^{-14}\,m^{-2/3}$. The ground station site is next to Madrid ($h_0 = 864\,m$) and the position of the GEO satellite is at 19.2^o East ($H = 36000\,km$). Wind speeds: $v = 10\,m/s$ (solid red line), $v = 21\,m/s$ (dashed green line), and $v = 30\,m/s$ (dashed-dotted line).*

$\delta = \{0, 15, 25, 40\}$ %. Note that the time-packed symbol time for the case of δ=0% collapses to the Nyquist symbol-time. The modulation of the optical feeder links is 4-PAM since it is used Intensity Modulation/Direct Detection scheme. On the contrary, the access link uses QPSK modulation which corresponds to the NB-IoT's one for the downlink. Therefore, in both links the number of modulation states is M=4 and the number of bits per modulated symbol is N_b=2.

In order to compare in a fair way all architectures they use the same data rate. Furthermore, it has not been considered an unique data rate but multiple ones. In particular, it has been tested the BLER and throughput of the aforementioned cases for nine possible code rates. Three code rates lower than the mother code rate of the convolutional encoding (*i.e.*, 0.2222, 0.259, and 0.3), three medium code rates (*i.e.*, 0.4444, 0.5319, and 0.6) and three high code rates (*i.e.*, 0.6386, 0.7678 and 0.854). For the first and second use cases these code rates correspond to the code rate of the NB-IoT waveform. However, for the third case, these code rates represent the joint code rate of the DVB-S2(X) and NB-IoT waveforms. This joint code rate is defined as the product between the code rates of the DVB-S2(X) and NB-IoT signals as

$$R_{c_{Case\ 3}} = R_{c_{NB\text{-}IoT}} \times R_{c_{DVB\text{-}S2(X)}}. \tag{32}$$

In (32) it has been selected the code rates of NB-IoT and DVB-S2(X) such that the their joint code rate, i.e. $R_{c\text{Case3}}$, is equal to the code rates of NB-IoT for the first and second cases. Thus, it has been considered three code rates (i.e. low, medium and high) for each waveform (i.e. NB-IoT and DVB-S2(X)) which permit to obtain the nine code rates for cases 1 and 2. Specifically, the used code rates of the DVB-S2(X) and NB-IoT are: $R_{c_{DVB-S2(X)}}$={0.66667, 0.8, and 0.9} [17] and $R_{c_{NB-IoT}}$={0.3333, 0.66667, and 0.96} respectively. Thus we obtain nine possible combinations of the code rates being the equivalent code rates among all transmission architectures (see Table 3 for more details).

So, after obtaining a similar code rate for the three cases under study, it will be determined the architecture that provides the best performance in terms of BLER and Throughput in terms of the uplink and downlink SNRs. Regarding the Throughput, it has been used the following expression for measuring it:

$$THR(\delta, R_c) = \frac{N_b \cdot R_c \cdot (1 - BLER)}{(1 + \rho) \cdot (1 - \delta)}, \tag{33}$$

Preprints (www.preprints.org) | NOT PEER-REVIEWED | Posted: 25 March 2021 doi:10.20944/preprints202103.0642.v1

Table 3. NB-IoT and DVB-S2(X) equivalent code rates for the relaying architectures under analysis.

$R_{cDVB-S2(X)}$	$R_{cNB-IoT}$	R_{cCase3}	$R_{cCase1and2}$
0.66667	0.33333	0.2222	0.2222
0.8	0.33333	0.2667	0.259
0.9	0.33333	0.3	0.3
0.66667	0.66667	0.4444	0.4444
0.8	0.66667	0.5333	0.5319
0.9	0.66667	0.6	0.6
0.66667	0.96	0.64	0.6386
0.8	0.96	0.768	0.7678
0.9	0.96	0.864	0.8628

Table 4. Maximum achievable throughput in terms of the overlapping factor and code rate.

R_c	$\delta = 0\%$	$\delta = 15\%$	$\delta = 25\%$	$\delta = 40\%$
0.2222	0.3864	0.4546	0.5152	0.6441
0.2590	0.4504	0.5299	0.6006	0.7507
0.3000	0.5217	0.6138	0.6957	0.8696
0.4444	0.7729	0.9093	1.0305	1.2881
0.5319	0.9250	1.0883	1.2334	1.5417
0.6000	1.0435	1.2276	1.3913	1.7391
0.6386	1.1106	1.3066	1.4808	1.8510
0.7678	1.3353	1.5709	1.7804	2.2255
0.8628	1.5005	1.7653	2.0007	2.5009

where in (33) the code rate R_c for the two first cases under study corresponds to the code rate of the NB-IoT waveform. For the third case, the value of R_c represents the joint code rate of the NB-IoT and DVB-S2(X) waveforms, which has been formulated in (32). The roll-off will be left constant for all simulations and equal to $\rho = 0.15$. Thus, according to the possible overlapping factors and code rates, the maximum achievable throughput can be obtained (see Table 4 for further details).

This maximum achievable throughput may not been achieved due to the presence of a residual time-packing interference, optical channel variation, and the noise in the uplink and feeder link may increase the BLER. So, simulation results will provide information about the transmission structure that provides the best performance in terms of BLER and Throughput. Note that low code rates provide very low BLER but the worse results in terms of throughput. On the contrary, high code rates may provide the highest achievable throughput but the worse BLER. For that reason it has been considered the BLER of 10^{-2} as the target BLER according to 5G specifications for providing normal services. This helps to decide the best transmission architecture. The case that satisfies the target BLER and provides the best throughput will be the best transmission architecture. Consequently, it is a mix between BLER and throughput. However, in order to compare the three cases under study is necessary to define additional figures of merit. The following section defines them.

4.3. Definition of the Figures of merit.

From previous section we have defined the throughput in terms of the overlapping factor and code rate. However, in the evaluation process of the three cases will be interested in the envelope of the throughput defined in (33). Specifically, we will be interested in the envelope of the throughput when it is left constant the overlapping factor. This throughput, denoted as $THR(\delta)^*$, is defined as the maximum throughput for all code rates with the same overlapping factor and it is computed as:

$$THR(\delta)^* = \max_{\mathbf{R_c}} \{THR(\delta, \mathbf{R_c})\}. \tag{34}$$

Preprints (www.preprints.org) | NOT PEER-REVIEWED | Posted: 25 March 2021 doi:10.20944/preprints202103.0642.v1

Next we will be interested in determining the throughput's envelope for the no-time and time packing schemes. For the case of no-time packing, the envelope of its throughput, denoted as THR_{NTP}, is obtained by particularizing (34) for δ=0, i.e. $THR_{NTP} = THR(\delta = 0)^*$. For the case of time-packing, its throughput's envelope, denoted as THR_{TP}, will be determined by computing the maximum of (34) for all overlapping factors higher than zero, δ>0, as follows:

$$THR_{TP} = \max_{\delta>0}\{THR(\delta)^*\}. \tag{35}$$

Then, the total throughput's envelope for a particular case will be obtained from the maximum envelope's throughput of the time-packed and non-time packed ones as:

$$THR_{Case\ q} = \max\{THR_{NTP}, THR_{TP}\}. \tag{36}$$

After defining alternative the envelope's of the throughput, we introduce two measures relatives to the gains in throughput. The first one measures if using time-packing is beneficial respect to non-time-packing. It provides a percentage of gain in throughput, denoted as $G_{THR}(\%)$, and it is computed as:

$$G_{THR}(\%) = \frac{(THR_{TP} - THR_{NTP}) \times 100}{THR_{NTP}}. \tag{37}$$

The second gain in throughput is related about measuring the best system. From the three cases, the first one it is the simplest one since the satellite does not manipulate it. So, it has been considered as the benchmark system. Then, it will be computed the relative gain of cases 2 and 3 respect to case 1. This gain is denoted as $\Delta G_{THRq,1}(\%)$, which represents the gain in envelope of case q, with $q \in \{2, 3\}$ respect to case 1. Also it is given in percentage and it is formulated as:

$$\Delta G_{THRq,1}(\%) = \frac{(THR_{Case\ q} - THR_{Case\ 1}) \times 100}{THR_{Case\ 1}}, \tag{38}$$

being $THR_{Case\ q}$ and $THR_{Case\ 1}$ the throughput's envelope for all cases under study computed following (36). Finally, after defining the figures of merit for analyzing the simulation results, we present the obtained results in the next section.

4.4. Simulation Results

The results provided in this section evaluate the BLER and Throughput of the three aforementioned architectures in the following aspects:

1. Evaluation the end-end BLER and Throughput when the E_b/N_0 of the feeder links varies from 2 to 22 dB in steps of 1 dB (see Fig. 9), the SNR of the access link is 20 dB, the wind speed of the clouds is 21 m/s, and the NB-IoT code rates are: $\mathbf{R}_{\mathbf{c_{NB-IoT}}}$={0.3333, 0.66667 and 0.95556}. There is no time-packing (*i.e.*, $\delta = 0\%$) and the tested configuration is case 1 (*i.e.*, Detect-and-Forward NB-IoT). The throughput of Fig. 9 is the $THR(\delta = 0, \mathbf{R}_{\mathbf{c_{NB-IoT}}})$ of (33).

2. Evaluation the end-end Throughput and BLER when the E_b/N_0 of the access links varies from -8 to 12 dB in steps of 1 dB (see Fig. 10), the SNR of the feeder link is 15, 20 and 25 dB, the wind speed is $v = 10, 21$ and 30 m/s, and the NB-IoT code rates are: $\mathbf{R}_{\mathbf{c_{NB-IoT}}}$={0.3333, 0.66667 and 0.95556}. There is no time-packing (*i.e.*, $\delta = 0\%$) and the tested configuration is the use case 1, *i.e.* Detect-and-Forward NB-IoT. The throughput of Fig. 10 is the $THR(\delta = 0, \mathbf{R}_{\mathbf{c_{NB-IoT}}})$ of (33).

3. Evaluation of the Throughput (see Fig. 11) and BLER (see Fig. 17) and for the Case 1: Detect-and-Forward NB-IoT when the SNR of the feeder link is 15 dB, the E_b/N_0 of the access varies from -8 to 12 dB, and the code rates of the NB-IoT and overlapping factors defined in Section 4.2. The throughput of Fig. 11 corresponds to $THR(\mathbf{delta}, \mathbf{R}_{\mathbf{c_{NB-IoT}}})$ of (33).

Preprints (www.preprints.org) | NOT PEER-REVIEWED | Posted: 25 March 2021 doi:10.20944/preprints202103.0642.v1

4. Evaluation of the Throughput (see Fig. 12) and BLER (see Fig. 18) and for the Case 2: Decode-and-Forward NB-IoT when the SNR of the feeder link is 15 dB, the SNR of the access varies from 0 to 20 dB, and the code rates of the NB-IoT and overlapping factors defined in Section 4.2. The throughput of Fig. 12 corresponds to $THR(\mathbf{delta}, \mathbf{R}_{\mathbf{c_{NB-IoT}}})$ of (33).

5. Evaluation of the Throughput (See Fig. 14) and BLER (See Fig. 19) and for the Case 3: Detect-and-Forward NB-IoT encapsulated in DVB-S2(X) frames when the SNR of the feeder link is 15 dB, the SNR of the access varies from 0 to 20 dB, and the code rates of the DVB-S2(X) and NB-IoT and overlapping factors defined in section 4.2. The throughput of Fig. 14 corresponds to $THR(\mathbf{delta}, \mathbf{R}_{\mathbf{c_{NB-IoT}}})$ of (33).

6. Evaluation of the Throughput's envelope when it is left constant the overlapping factor for all cases under study (See Fig. 13a,13b,13c) when the SNR of feeder link is 15 dB, the SNR of the access varies from 0 to 20 dB, and the code rates of the DVB-S2(X) and NB-IoT and overlapping factors defined in section 4.2. The throughput of these figures corresponds to $THR(\delta)^*$ of (34).

7. Evaluation of the gain in throughput using time-packing respect to no-time packing is shown in Fig. 13d. The SNR of feeder link is 15 dB, the SNR of the access varies from 0 to 20 dB. This gain is denoted as $G_{THR}(\%)$ and computed following (37).

8. Comparison among Envelope of the Throughput for all cases under study (See Fig. 15a,15b,15c,15d) in terms of the overlapping factor, when the SNR of feeder link is 15 dB, the SNR of the access varies from 0 to 20 dB, and the code rates of the DVB-S2(X) and NB-IoT and overlapping factors defined in section 4.2. The throughput of these figures corresponds to $THR(\delta)^*$ of (34).

9. Comparison of the envelope of the Throughput for all cases under study (See Fig. 16a) when the SNR of feeder link is 15 dB, the SNR of the access varies from 0 to 20 dB. The throughput plotted in this figure is denoted as $THR_{Case\ q}$ and computed according to (36).

10. Comparison of the gain in throughput that offer cases 2 and 3 respect to case 1 (See Fig. 16b) when the SNR of feeder link is 15 dB, the SNR of the access varies from 0 to 20 dB. This gain in throughput of this figure is denoted as $\Delta G_{THRq,1}$ with $q \in \{2, 3\}$, and determined following (38).

Preprints (www.preprints.org) | NOT PEER-REVIEWED | Posted: 25 March 2021 doi:10.20944/preprints202103.0642.v1

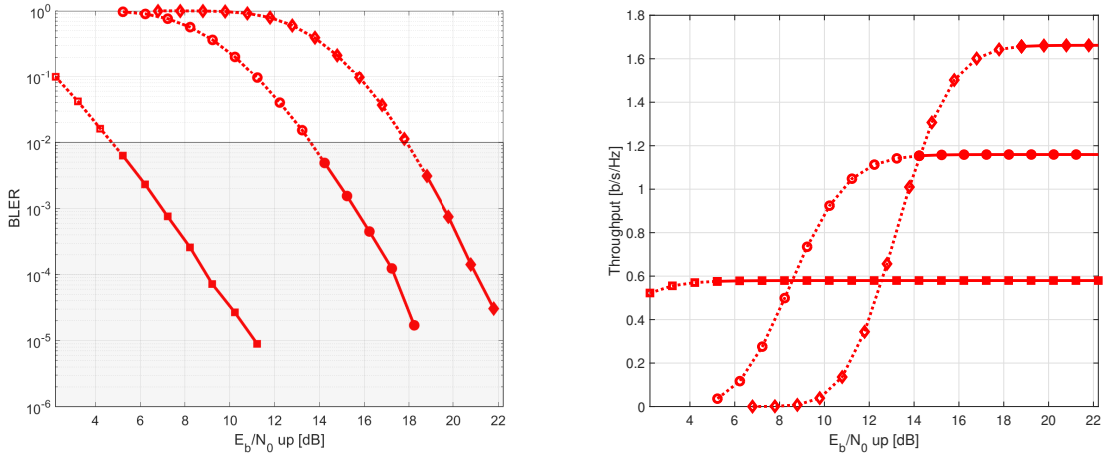

(a) *BLER for* $\delta = 0\,\%$. SNR_{down}=*20 dB*

(b) *Throughput for* $\delta = 0\,\%$. SNR_{down}=*20 dB*

Figure 9. *End-to-end BLER (left) and throughput (right) versus* E_b/N_0 *in the access link for a NB-IoT frame* ($SNR_{\text{access}} = 20$ *dB). NB-IoT code rates:* 0.33333 *(square),* 0.66667 *(circle),* 0.95556 *(diamond), when the wind speed is* $v = 21$ *m/s. Solid lines with filled markers: BLER* 10^{-2} *requirement fulfilled. Dashed-lines with unfilled markers: BLER* 10^{-2} *requirement not fulfilled.Diameter of aperture's telescope:* $W_0 = 21$ *cm.*

From the simulations of the end-end BLER and Throughput in terms of the SNR of the uplink for a very high SNR of the access link, (See Fig. 9), then it is possible to observe region in which the uplink limits the transmission. In all plots the dotted lines means that the BLER is higher than the target BLER whereas the continuous ones represent that their BLER is lower than the target BLER, i.e. 0.01. For a better indication, the grey area in the figure of BLER show the region of SNRs for which the tested code rates for NB-IoT satisfies the target BLER. Thus, it is possible to observe that the code rate of Rc_{NB-IoT}=0.3333 provides the best throughput when the SNR of the feeder link is ranged between 13 and 19 dB, Rc_{NB-IoT}=0.6666 is the best option when the feeder's link SNR is between 19 and 22 dB, and finally Rc_{NB-IoT}=0.95556 is the best one when the uplink SNR is larger than 22 dB. According to this result we have chosen the SNR of the feeder link of 15, 20 and 25 dB for determining the degradation of the end-end link in terms of the wind speed.

Fig. 10 evaluates the degradation of the BLER (Figures at the left) and throughput (Figures at the right) when the wind speed is 10, 21, 30 m/s for the uplink SNRs of 15, 20, and 25 dB. Simulation results show that the higher is the SNR of the feeder link, the lower is the degradation of the end-end BLER and Throughput due to the wind speed of the clouds. Consequently, it has been motivated to use the SNR of 15 dB as the reference SNR for using in the feeder link in the comparison of the three satellite architectures.

Preprints (www.preprints.org) | NOT PEER-REVIEWED | Posted: 25 March 2021 doi:10.20944/preprints202103.0642.v1

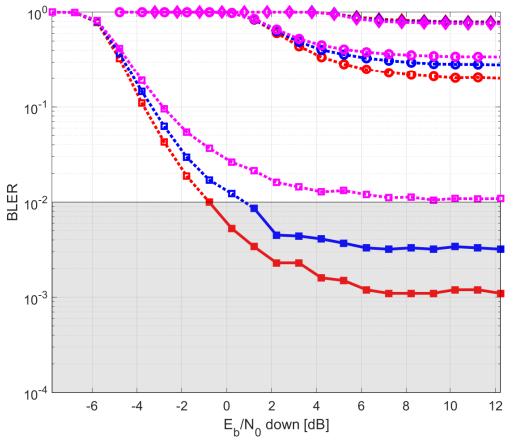

(a) *BLER for* $\delta = 0\,\%$. SNR_{up}=*15 dB*

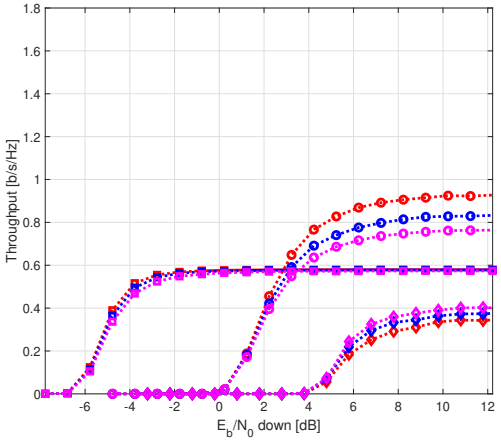

(b) *Throughput for* $\delta = 0\,\%$. SNR_{up}=*15 dB*

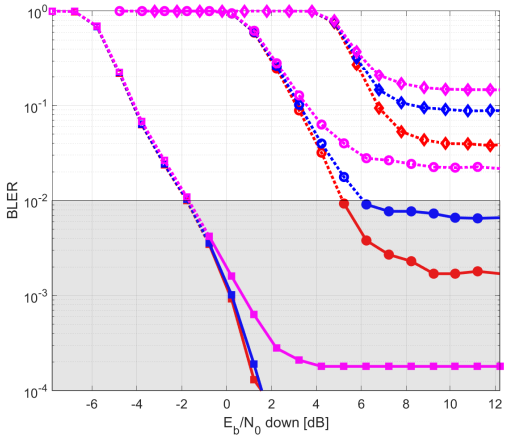

(c) *BLER for* $\delta = 0\,\%$. SNR_{up}=*20 dB*

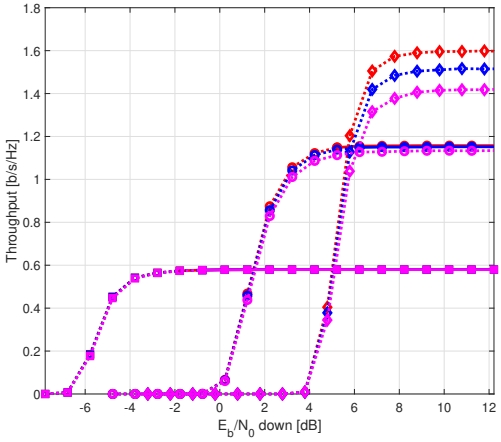

(d) *Throughput for* $\delta = 0\,\%$. SNR_{up}=*20 dB*

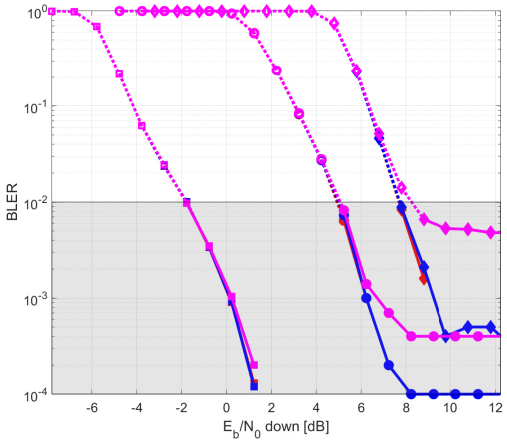

(e) *BLER for* $\delta = 0\,\%$. SNR_{up}=*25 dB*

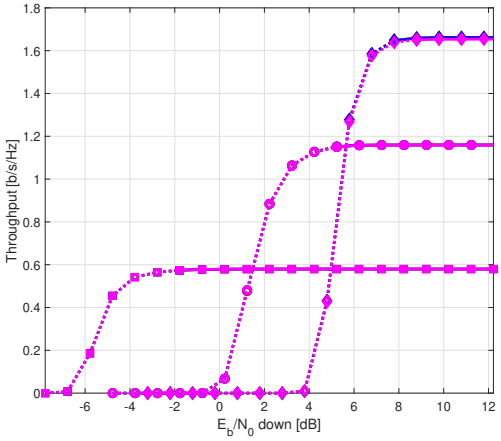

(f) *Throughput for* $\delta = 0\,\%$. SNR_{up}=*25 dB*

Figure 10. *End-to-end BLER (left) and throughput (right) versus* E_b/N_0 *in the access link for a NB-IoT frame (*$SNR_{\text{feeder}} = 15$, *20 and 25 dB). NB-IoT code rates:* 0.33333 *(square),* 0.66667 *(circle),* 0.95556 *(diamond), when the wind speed is* $v = 10$ *m/s (red),* $v = 21$ *m/s (blue) and* $v = 30$ *m/s (magenta). Solid lines with filled markers: BLER* 10^{-2} *requirement fulfilled. Dashed-lines with unfilled markers: BLER* 10^{-2} *requirement not fulfilled.Diameter of aperture's telescope:* $W_0 = 10$ *cm.*

Preprints (www.preprints.org) | NOT PEER-REVIEWED | Posted: 25 March 2021 doi:10.20944/preprints202103.0642.v1

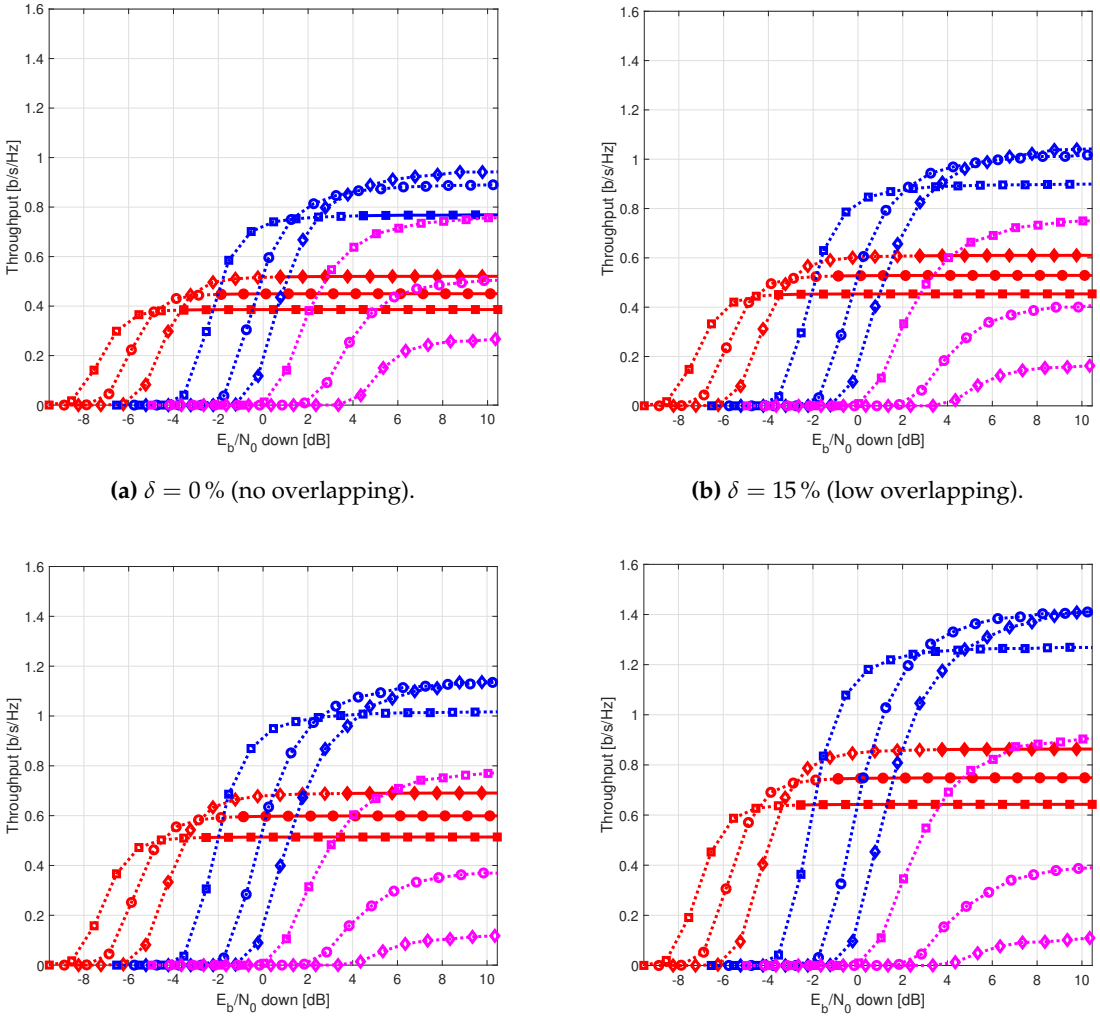

(a) $\delta = 0\,\%$ (no overlapping).

(b) $\delta = 15\,\%$ (low overlapping).

(c) $\delta = 25\,\%$ (medium overlapping).

(d) $\delta = 40\,\%$ (high overlapping).

Figure 11. *End-to-end throughput versus* E_b/N_0 *in the access link for a NB-IoT frame (*$SNR_{\text{feeder}} = 15\,dB$*). NB-IoT code rates:* 0.2222 *(red square),* 0.259*(red circle),* 0.3 *(red diamond),* 0.444 *(blue square),* 0.5319 *(blue circle),* 0.6 *(blue diamond),* 0.6386 *(magenta square),* 0.7678 *(magenta circle),* 0.8628 *(magenta diamond). Solid lines with filled markers: BLER* 10^{-2} *requirement fulfilled. Dashed-lines with unfilled markers: BLER* 10^{-2} *requirement not fulfilled. Wind speed:* $v = 21$ *m/s and diameter of aperture's telescope:* $W_0 = 10$ *cm.*

Fig. 11 shows the throughput for each overlapping factor and code rate, whereas Fig. 13a plots the envelope's throughput for all overlapping factor for the case 1: Detect-and-forward with NB-IoT. Simulation results show that the unique segment of NB-IoT code rates that satisfies the target BLER is the lowest one, *i.e.*, $R_{c_{NB-IoT}}$={0.2222, 0.259, and 0.3} for all time-packing overlapping. The medium code rate of $R_c = 0.4444$ is able to achieve its maximum throughput only when there is no overlapping (*i.e.* $\delta = 0\%$). The other code rates (i.e. medium and larger) are mainly penalized by the SNR of the uplink and are not able to achieve their maximum throughput (see Table 4). If we compare the performance of time-packing schemes vs no-time-packing ones, results show that in all cases time-packing schemes show a better throughput than the non-time packed ones. However, the gain in throughput strongly depends on the E_b/N_0 of the access. Towards this regard, Fig. 13d shows the % of gain in throughput of the time-packed vs no time-packed signalling. There it is possible to observe that for the set of E_b/N_0 ranged between -2 and 5 dB the gain in envelope's throughput of time-packed schemes versus

Preprints (www.preprints.org) | NOT PEER-REVIEWED | Posted: 25 March 2021 doi:10.20944/preprints202103.0642.v1

no-time-packed ones is around 50% of average. For other values of E_b/N_0 the % of gain in throughput falls down to only a 10%.

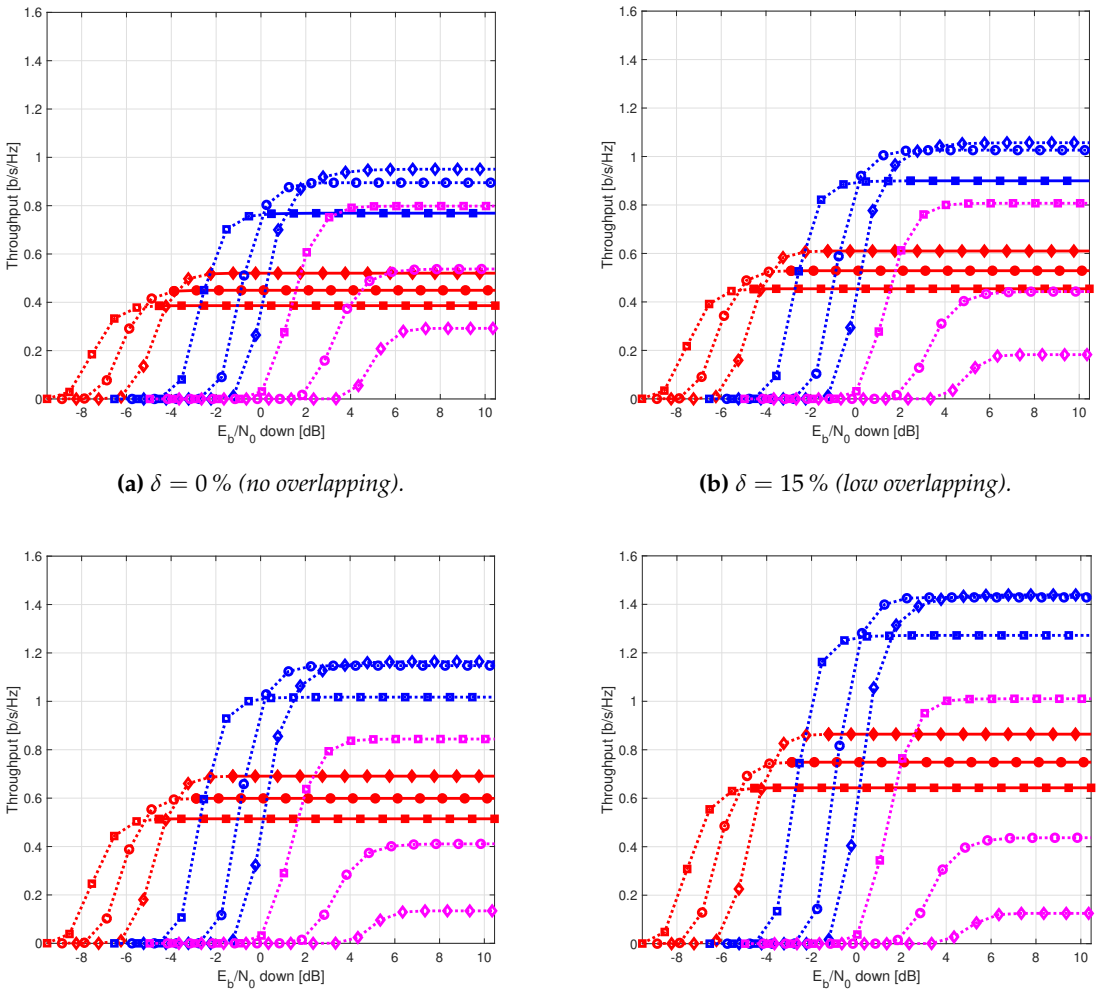

(a) $\delta = 0\,\%$ *(no overlapping).*

(b) $\delta = 15\,\%$ *(low overlapping).*

(c) $\delta = 25\,\%$ *(medium overlapping).*

(d) $\delta = 40\,\%$ *(high overlapping).*

Figure 12. *End-to-end throughput versus* E_b/N_0 *in the access link for a NB-IoT frame in a regenerative satellite (decode forward)* ($SNR_{\text{feeder}} = 15\,dB$). *NB-IoT code rates:* 0.2222 *(red square),* 0.259 *(red circle),* 0.3 *(red diamond),* 0.444 *(blue square),* 0.5319 *(blue circle),* 0.6 *(blue diamond),* 0.6386 *(magenta square),* 0.7678 *(magenta circle),* 0.8628 *(magenta diamond). Solid lines with filled markers: BLER* 10^{-2} *requirement fulfilled. Dashed-lines with unfilled markers: BLER* 10^{-2} *requirement not fulfilled. Wind speed:* $v = 21$ *m/s and diameter of aperture's telescope:* $W_0 = 10$ *cm.*

Similarly to case 1, Fig. 12, Fig. 13b and Fig. 13d show the throughput for each code rate and overlapping factor, envelope's throughput for each overlapping factor and the % in gain of throughput of time-packed schemes vs no time packed ones for case 2: decode-and-forward NB-IoT. From Fig. 12 it is possible to observe that the regeneration of the NB-IoT signal at the satellite permits to use also medium code rates with time-packing of δ={0,15}%, i.e. $R_{c_{NB-IoT}}$=0.4444. So, it means that the largest throughput is not obtained with the largest overlapping factor (i.e. δ=40%) and low code rates (i.e. $R_{c_{NB-IoT}}$=0.3) as in the previous case, but with moderate overlapping factors (i.e. δ=15%) and medium code rates (i.e. $R_{c_{NB-IoT}}$=0.4444). If we compare the % of the envelope's throughput of the time-packed schemes vs no time-packed ones, we observe that also this gain strongly depends of the E_b/N_0 of the access link. Specifically, from Fig. 13d we can conclude that for E_b/N_0 ranged between -4 and 1 dB, the

Preprints (www.preprints.org) | NOT PEER-REVIEWED | Posted: 25 March 2021 doi:10.20944/preprints202103.0642.v1

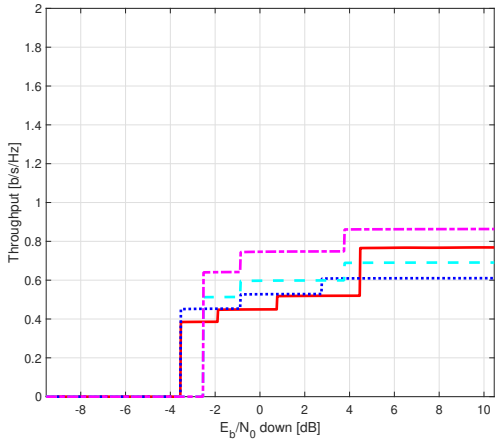

(a) *Envelope of Throughput Case 1*

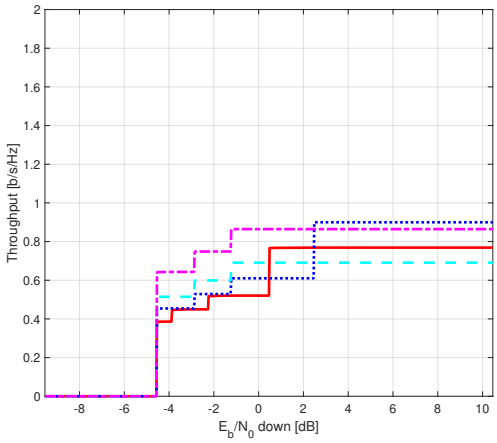

(b) *Envelope of Throughput Case 2*

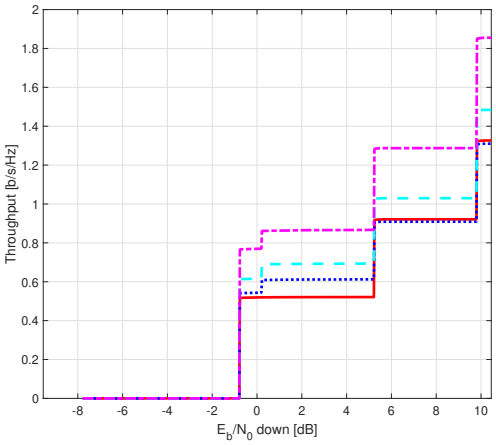

(c) *Envelope of Throughput Case 3*

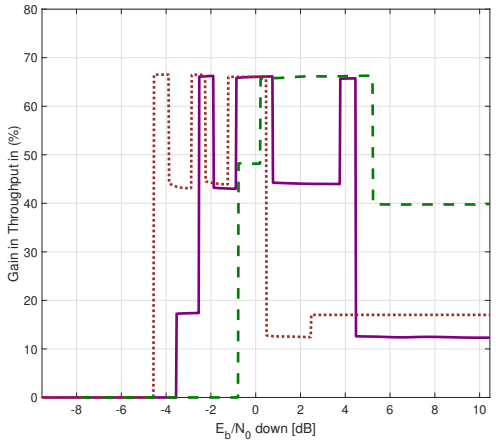

(d) *Gain in Throughput all cases*

Figure 13. *End-to-end envelope of throughput (left-hand side), and end-to-end gain in the envelope of throughput of time-packed vs. no-time-packed (right-hand side), represented as function of the* E_b/N_0 *in the access link for case 3). Overlapping of* $\delta = 0\%$ *(solid red line),* $\delta = 15\%$ *(dotted blue line),* $\delta = 25\%$ *(dashed cyan line), and* $\delta = 40\%$ *(dashed-dotted magenta line). Sub-figure 13d shows the gain in throughput of time-packed with respect to no-time-packed; here, case 1) is represented in continuous purple line, case 2) is plotted in dotted brown line, and case 3) is shown in dashed green line. Wind speed:* $v = 21$ *m/s; Beam width:* $W_0 = 10$ *cm.*

% gain in throughput of time-packed schemes is larger that 40%. On the contrary, for E_b/N_0 larger than 1 dB, the % gain in throughput falls down to around 20%.

Next, Fig. 14, Fig. 13c and Fig. 13d plot the throughput in terms of the code rate for each overlapping factor, envelope's throughput for each overlapping factor and % of gain in throughput for the time-packed vs no-time packed schemes respectively for the case 3: decoded DVB-S2(X) and detect-and-forward NB-IoT. Fig. 14 shows that the best option is to use in optical feeder link a code rate $R_{c_{DVB-S2X}}$=0.6666. For the NB-IoT system the best option is to use a $R_{c_{NB-IoT}}$=0.3333, for an E_b/N_0 ranged between -1 and 5 dB, a $R_{c_{NB-IoT}}$=0.66666, for an E_b/N_0 between -5 and 9 dB, and $R_{c_{NB-IoT}}$=0.96 for E_b/N_0 larger than 9 dB. Regarding the envelope's throughput for all overlapping factors, Fig. 13c indicates that similarly to case 1, it is better to use the largest overlapping factor (i.e.δ=40%) to obtain the highest throughput. If we compare the throughput that provide the time-packed and no-time

Preprints (www.preprints.org) | NOT PEER-REVIEWED | Posted: 25 March 2021 doi:10.20944/preprints202103.0642.v1

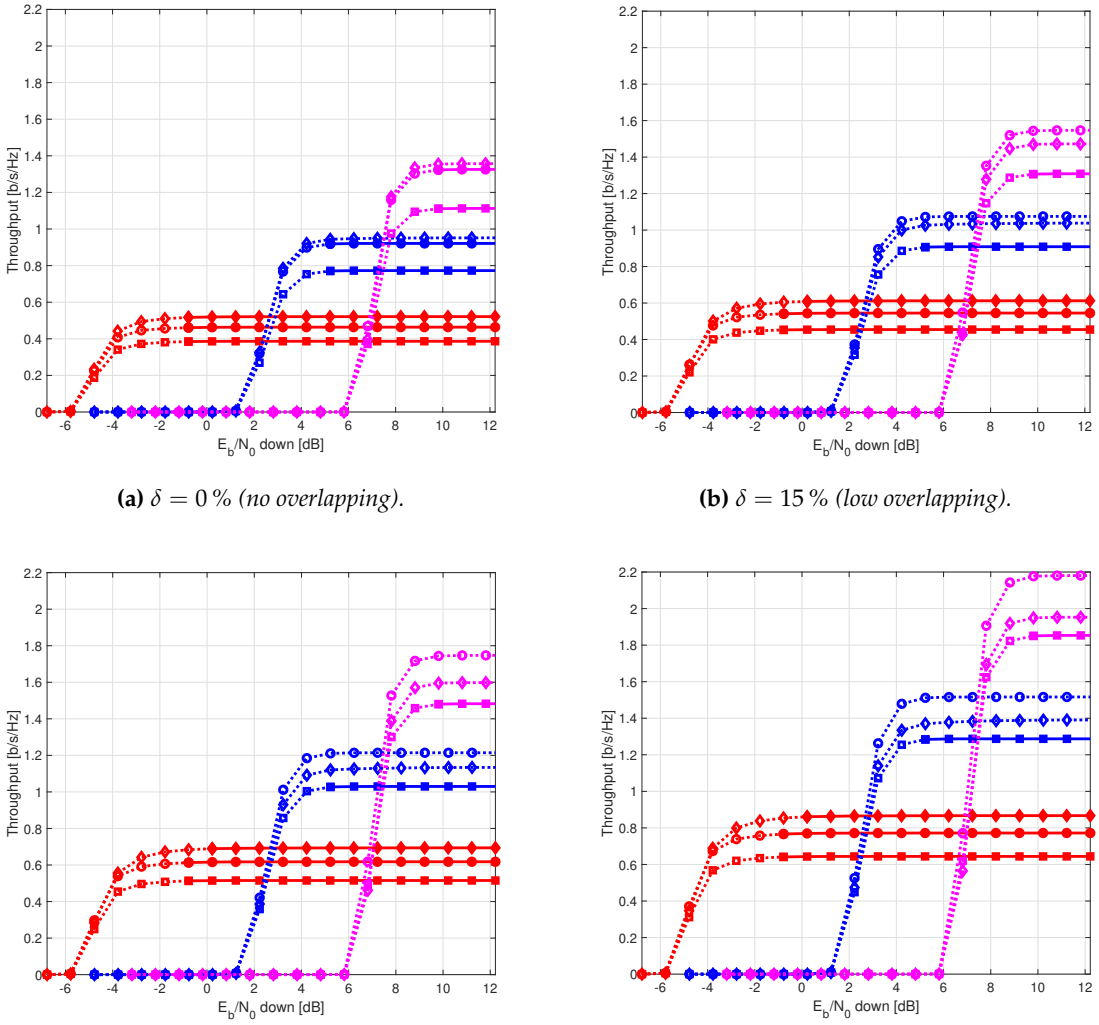

(a) $\delta = 0\,\%$ *(no overlapping).*

(b) $\delta = 15\,\%$ *(low overlapping).*

(c) $\delta = 25\,\%$ *(medium overlapping).*

(d) $\delta = 40\,\%$ *(high overlapping).*

Figure 14. *End-to-end throughput versus* E_b/N_0 *in the access link for a NB-IoT frame encapsulated in a DVB-S2(X) satellite frame (*$SNR_{\text{feeder}} = 15\,dB$*). NB-IoT code rates:* 1/3 *(red),* 2/3 *(blue),* 0.96 *(magenta). DVB-S2(X) code rates:* 2/3 *(squares),* 0.8 *(circles),* 0.9 *(diamonds). Solid lines with filled markers: BLER* 10^{-2} *requirement fulfilled. Dashed-lines with unfilled markers: BLER* 10^{-2} *requirement not fulfilled. Wind speed:* $v =$ 21 *m/s and diameter of aperture's telescope:* $W_0 = 10$ *cm.*

packed configurations, we observe from Fig. 13d that for an E_b/N_0 larger than 0 dB is obtained a minimum gain in throughput of 40%. Consequently, this case compared with the previous ones, provides the largest gain in throughput when comparing time-packed vs no-time packed ones. However, the minimum E_b/N_0 from which it is better to use time-packing is larger than in the other two previous cases.

Fig. 15 shows the envelope of the throughput for all cases in terms of the overlapping factor. From these figures it is possible to observe that for cases 1 and 3 the larger the overlapping factor, the larger the maximum throughput (i.e. $\delta = 40\%$). On the contrary for case 2, the maximum throughput is achieved when the overlapping factor is $\delta = 15\%$.

Preprints (www.preprints.org) | NOT PEER-REVIEWED | Posted: 25 March 2021 doi:10.20944/preprints202103.0642.v1

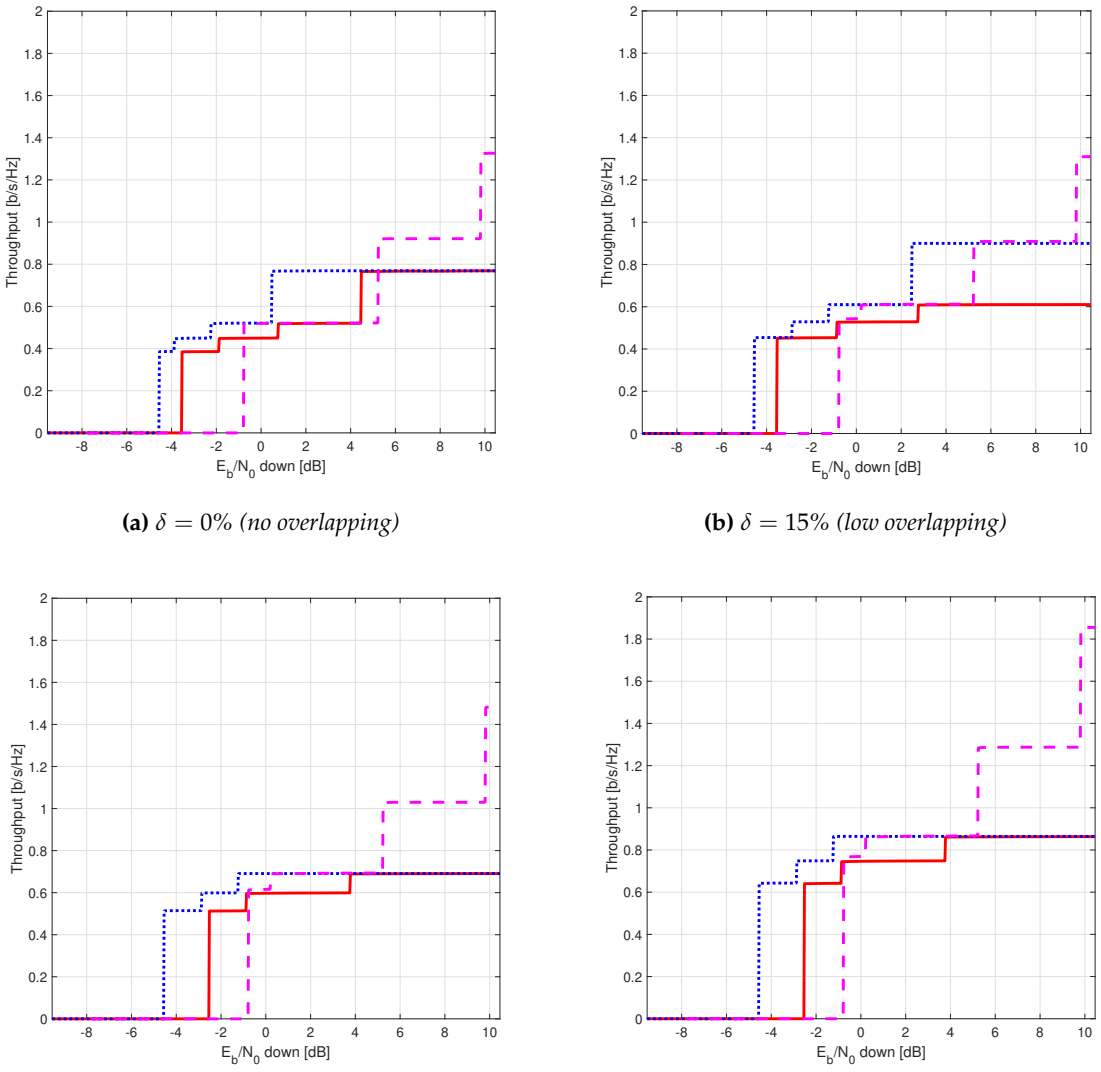

(a) $\delta = 0\%$ *(no overlapping)*

(b) $\delta = 15\%$ *(low overlapping)*

(c) $\delta = 25\%$ *(medium overlapping)*

(d) δ*=40% (high overlapping)*

Figure 15. *End-to-end envelope of throughput for all cases under study versus* E_b/N_0 *in the access link. Case 1 (continuous red line), Case 2 (dotted blue line) and Case 3 (dashed magenta line). Wind speed:* $v = 21$ *m/s and diameter of aperture's telescope:* $W_0 = 10$ *cm.*

Next, Fig. 16 plots the envelope of the throughput for all cases (Fig. 16a) and the % gain of cases 2 and 3 respect to case 1 (Fig. 16b). From Fig. 16a is possible to conclude that with independence of the overlapping factor, the cases 2 and 3 always have a better throughput than case 1. So, case 1 will be the benchmark case for determining the goodness of cases 2 and 3. Note also from this figure that the regeneration of the NB-IoT signal permits to lower the minimum E_b/N_0 around 1.5 dB and 4 dB respect to case 1 and 3 respectively. Regarding the gain in throughput of cases 2 and 3 respect to case 1, for E_b/N_0 lower than -2 dB the best option is to use case 2, for an E_b/N_0 ranged between -2 and 4 dB case 2 and 3 provide practically the same throughput. Finally, for E_b/N_0 larger than 4 dB the best strategy is to encapsulate the NB-IoT frames into the DVB-S2(X) ones (case 3).

Preprints (www.preprints.org) | NOT PEER-REVIEWED | Posted: 25 March 2021 doi:10.20944/preprints202103.0642.v1

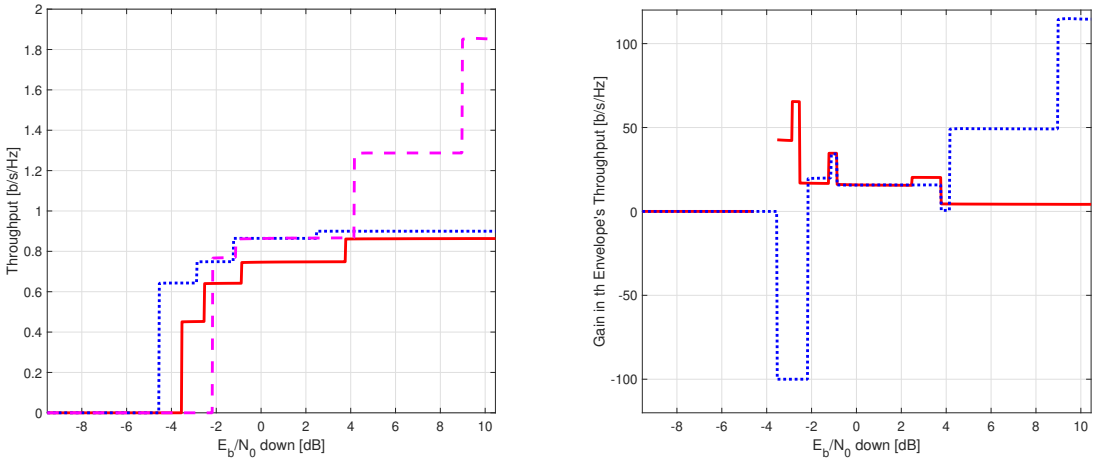

(a) *Envelope's throughput for all cases* **(b)** *Gain in throughput of cases 2 and 3 respect case 1*

Figure 16. *End-to-end envelope of throughput for all cases under study versus E_b/N_0 in the access link. Case 1 (continuous red line), Case 2 (dotted blue line) and Case 3 (dashed magenta line) (Left size). At the right size, gain in the end-to-ends throughput of cases 2 (continuous red line) and 3 (dashed blue line) respect case 1. Wind speed: v = 21 m/s and diameter of aperture's telescope: W_0 = 10 cm.*

5. Conclusions

The bottleneck of future mobile systems to implement OTA applications in a global scale, such as software and firmware updates for autonomous driving, is foreseen to the the feeder link of the satellite link. To tackle this issue, it has been considered to use optical wireless technologies in the feeder link, to satisfy the high data rate demand that will be required in the feeder link. Towards this regard, this paper presents the closed-form formulas that are needed to estimate the impairments that that are introduced in the uplink optical transmission in terms of the wind speed, wavelength of the optical signal, and beam width/telescope aperture, refractive index structure of the atmosphere, and azimuth angle of transmission, among others. Furthermore, it has been considered to use time-packing to increase the spectral efficiency of the optical feeder link even further. Finally, three different relaying strategies have been considered for the GEO satellite forward link: 1) Detect-and-Forward with NB-IoT; 2) Decode-and-Forward with NB-IoT; and 3) Decode-and-Forward with NB-IoT/DVB-S2(X). From the simulation results that were obtained, it was possible to conclude that the wind speed has little effect on the end-to-end performance for mean SNR values of more than 20 dB in the optical feeder link. For this reason, the performance of the different relaying strategies has been studied in further details for the optical feeder link at 15 dB (*i.e.*, 10 dB atmospheric loss in the proposed optical link budget).

In order to be fair with all the cases under study, comparisons have been made using the same code rate. For relaying architectures 1) and 2), these code rates corresponds to the ones defined in the NB-IoT standard. Nevertheless, for relaying architecture 3), the equivalent code rate is equal to the product between the code rates of the DVB-S2(X) and NB-IoT frames. This can be obtained by using two higher code rates. Simulation results showed that for relaying architecture 1), the highest throughput was obtained when using the lowest NB-IoT code rate (*i.e.*, $R_c = 0.3$) with the largest overlapping factor (*i.e.*, $\delta = 40\%$). On the contrary, for the relaying architecture 2), the highest throughput was reached when using medium code rates (*i.e.*, $R_c = 0.4444$) and medium values of overlapping factor (*i.e.*, $\delta = 15\%$). Finally, for the relaying architecture 3), the largest throughput was obtained when the DVB-S2(X) frame used a code rate of R_c=0.66667. The code rate of NB-IoT depends on the E_b/N_0 of the access links. Specifically, the NB-IoT has to use a $R_{cNB-IoT} = 0.3333$ for an E_b/N_0 ranged between -1 and 5 dB, a $R_{cNB-IoT} = 0.66666$ for an E_b/N_0 between -5 and 9 dB, and

Preprints (www.preprints.org) | NOT PEER-REVIEWED | Posted: 25 March 2021 doi:10.20944/preprints202103.0642.v1

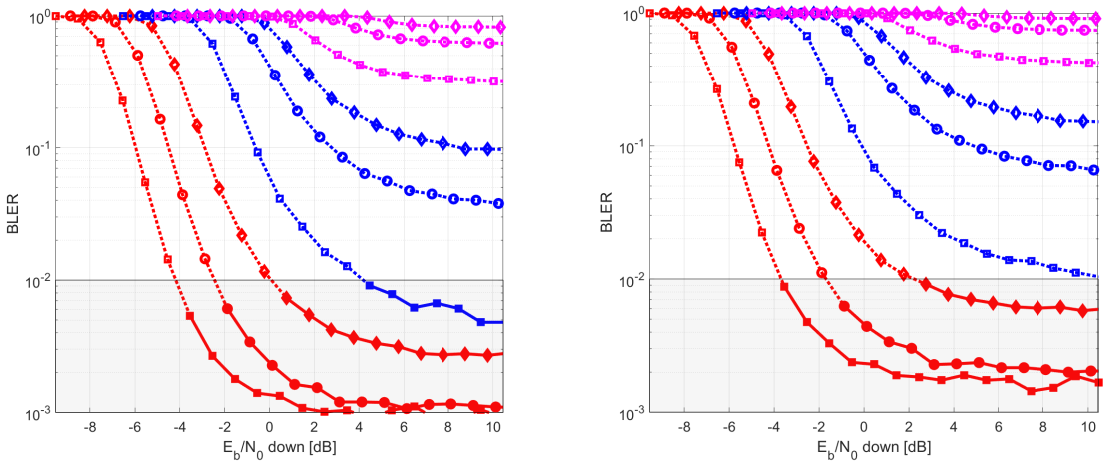

(a) $\delta = 0\,\%$ *(no overlapping).*

(b) $\delta = 15\,\%$ *(low overlapping).*

(c) $\delta = 25\,\%$ *(medium overlapping).*

(d) $\delta = 40\,\%$ *(high overlapping).*

Figure 17. *End-to-end Block Error Rate (BLER) versus* E_b/N_0 *in the access link for a NB-IoT frame* ($SNR_{\text{feeder}} = 15\,dB$). *NB-IoT code rates:* 0.2222 *(red square),* 0.259*(red circle),* 0.3 *(red diamond),* 0.444 *(blue square),* 0.5319 *(blue circle),* 0.6 *(blue diamond),* 0.6386 *(magenta square),* 0.7678 *(magenta circle),* 0.8628 *(magenta diamond). Solid lines with filled markers: BLER* 10^{-2} *requirement fulfilled. Dashed-lines with unfilled markers: BLER* 10^{-2} *requirement not fulfilled. Wind speed:* $v = 21\,m/s$; *Beam width:* $W_0 = 10\,cm$.

$R_{cNB-IoT} = 0.96$ for E_b/N_0 larger than 9 dB. Similarly to case 1), the higher the overlapping factor the larger the throughput that it is obtained.

Regarding the comparison of time-packed versus no time-packed signalling for the three relaying architectures under analysis, it was observed that the use of time-packing is beneficial in all cases. For case 1), it was possible to see that for E_b/N_0 ranged between -2 and 5 dB, the gain in the outer (envelope) throughput was in the order of 50% when comparing time-packed to no-time-packed performance. For other values of E_b/N_0 under study, the percent gain in throughput fell down notably to about 10%. For case 2), it was also observed that that the throughput gain depended strongly on the E_b/N_0 of the access link. Specifically, for E_b/N_0 ranged between -4 and 1 dB, the percent gain in throughput of time-packed schemes was larger that 40%. On the contrary, for E_b/N_0 larger than 1 dB, the percentage gain in throughput fell down to around 20%. Finally, for case 3), it was observed that for an E_b/N_0 larger than 0 dB, the minimum gain in throughput that was feasible was as high as 40 %. Consequently, this case compared with the previous ones, provides the largest gain in throughput

Preprints (www.preprints.org) | NOT PEER-REVIEWED | Posted: 25 March 2021 doi:10.20944/preprints202103.0642.v1

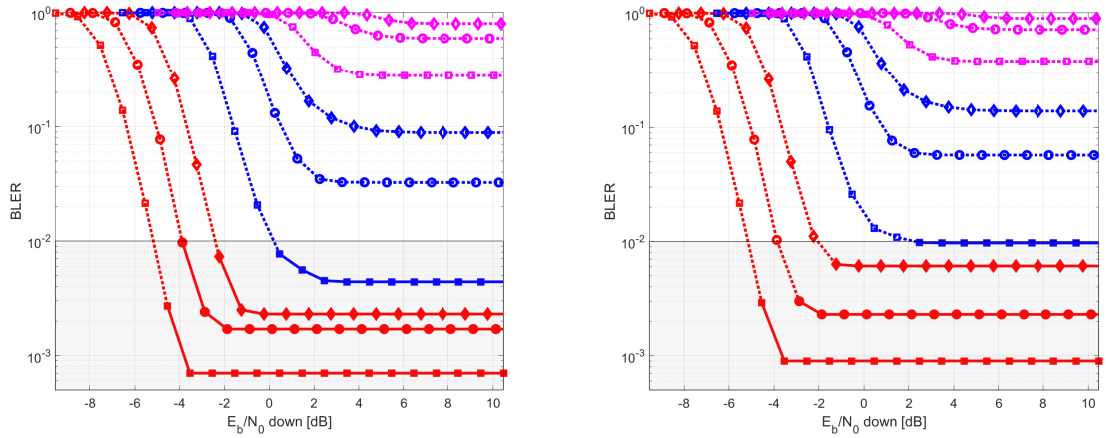

(a) $\delta = 0\,\%$ *(no overlapping).*

(b) $\delta = 15\,\%$ *(low overlapping).*

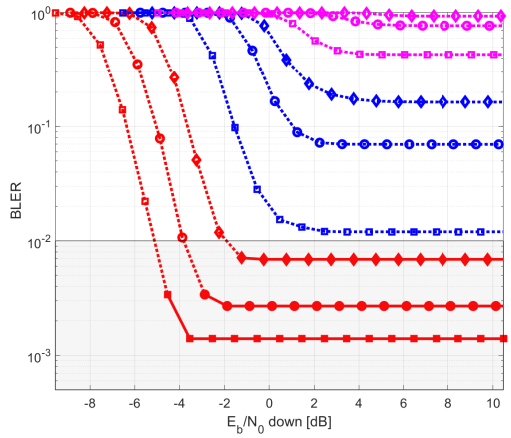

(c) $\delta = 25\,\%$ *(medium overlapping).*

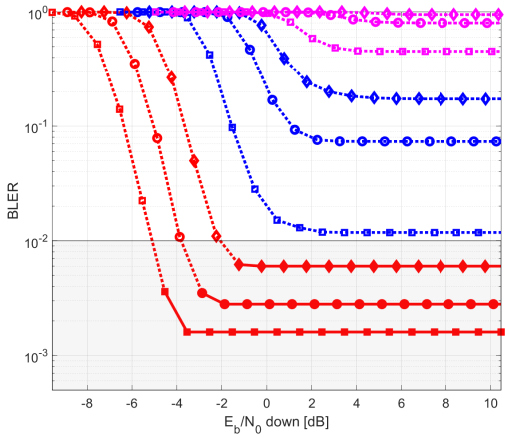

(d) $\delta = 40\,\%$ *(high overlapping).*

Figure 18. *End-to-end Block Error Rate (BLER) versus* E_b/N_0 *in the access link for a NB-IoT frame transmitted through regenerative satellite (decode forward) (*$SNR_{\text{feeder}} = 15\,dB$*).NB-IoT code rates:* 0.2222 *(red square),* 0.259*(red circle),* 0.3 *(red diamond),* 0.444 *(blue square),* 0.5319 *(blue circle),* 0.6 *(blue diamond),* 0.6386 *(magenta square),* 0.7678 *(magenta circle),* 0.8628 *(magenta diamond). Solid lines with filled markers: BLER* 10^{-2} *requirement fulfilled. Dashed-lines with unfilled markers: BLER* 10^{-2} *requirement not fulfilled. Wind speed:* $v = 21$ *m/s and diameter of aperture's telescope:* $W_0 = 10$ *cm*

when comparing time-packed vs no-time packed ones. However, the minimum E_b/N_0 from which it is better to use time-packing is larger than in the other two previous cases.

When the end-end throughput for all satellite relaying architectures were jointly compared, it was observed that case 2) and 3) are able to reach a higher throughput than case 1). Specifically, it was observed that for E_b/N_0 lower than -2 dB, the best option was to use case 2); then, for E_b/N_0 ranged between -2 and 4, both case 2) and 3) provided practically the same throughput with a gain in the order of 20% with respect case 1). Finally, for E_b/N_0 larger than 4 dB, the best strategy was to encapsulate the NB-IoT frames into the DVB-S2(X) frames, also known as relaying architecture 3), since it enabled a minimum gain in throughput in the order of 50% with respect to case 1). Note that case 2) regenerated the NB-IoT signal, whereas case 3) protected the NB-IoT symbols by introducing the code rate of DVB-S2(X). When the E_b/N_0 of the access link was low, then the LDPC decoder of DVB-S2(X) did not converge and, due to that, it introduced errors in the NB-IoT frames that were decoded on-board the satellite for retransmission in downlink. These NB-IoT frames were protected

Preprints (www.preprints.org) | NOT PEER-REVIEWED | Posted: 25 March 2021 doi:10.20944/preprints202103.0642.v1

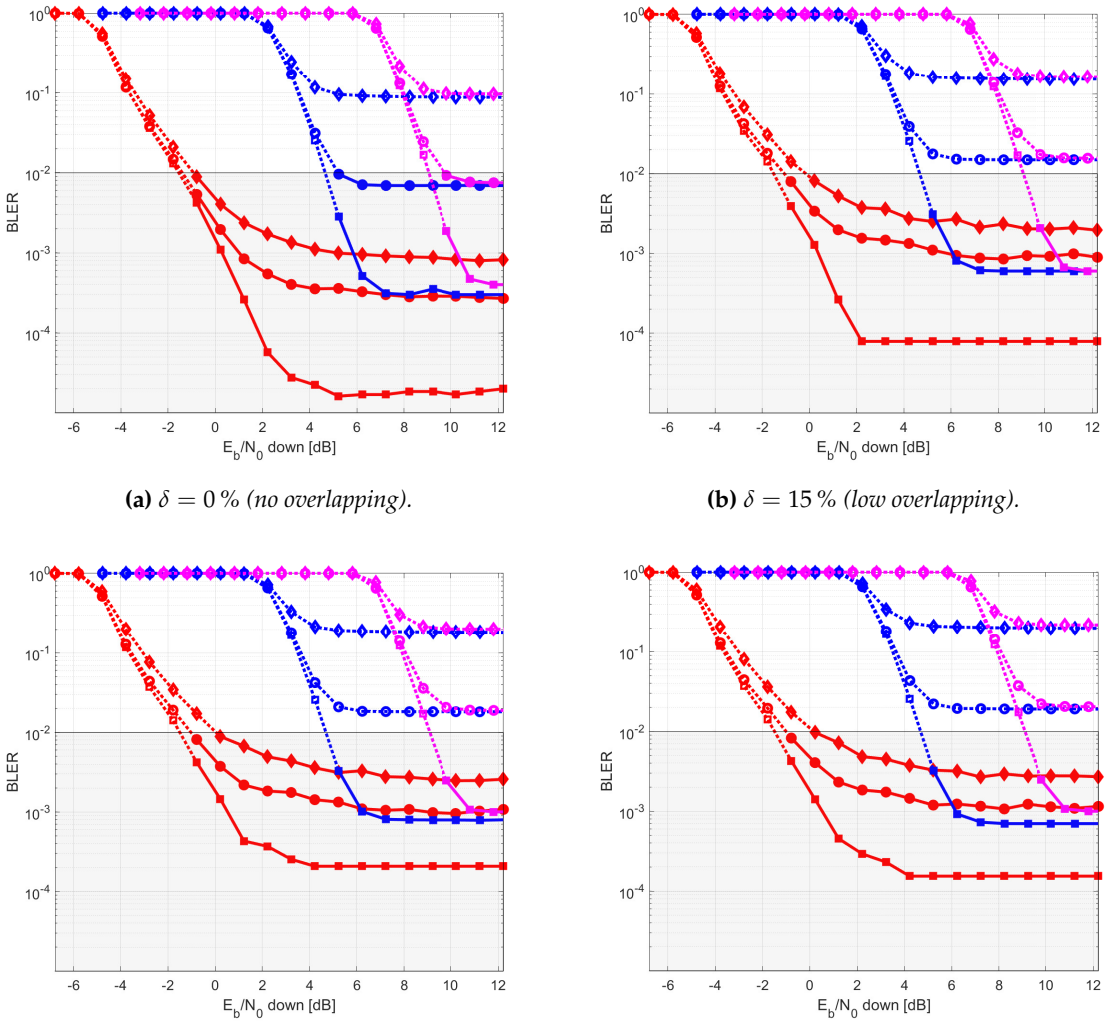

(a) $\delta = 0\,\%$ *(no overlapping).*

(b) $\delta = 15\,\%$ *(low overlapping).*

(c) $\delta = 25\,\%$ *(medium overlapping).*

(d) $\delta = 40\,\%$ *(high overlapping).*

Figure 19. *End-to-end Block Error Rate (BLER) versus* E_b/N_0 *in the access link for a NB-IoT frame encapsulated in a DVB-S2(X) satellite frame (*$SNR_{feeder} = 15\,dB$*). NB-IoT code rates:* 1/3 *(red),* 2/3 *(blue),* 0.96 *(magenta). DVB-S2(X) code rates:* 2/3 *(squares),* 0.8 *(circles),* 0.9 *(diamonds). Solid lines with filled markers: BLER* 10^{-2} *requirement fulfilled. Dashed-lines with unfilled markers: BLER* 10^{-2} *requirement not fulfilled. Wind speed:* $v =$ 21 *m/s and diameter of aperture's telescope:* $W_0 = 10$ *cm.*

with a code rate larger than their equivalent for the cases 1) and 2); therefore, it was expected that at low E_b/N_0, the case 3) strategy was not the optimum one. However, when the E_b/N_0 of the access increased, the LDPC decoder started to converge and, due to that, it managed to remove the erroneous bits that were introduced by the optical feeder link in the NB-IoT frames that were encapsulated in the DVB-S2(X) signal. Here, as the NB-IoT frames had a higher code rate than the code rates that were used for cases 1) and 2), it offered the largest throughput.

Consequently, the link layer should dynamically change the transmission architecture according to the E_b/N_0 of the access link. Therefore, it would be necessary a control channel from the NB-IoT terminals to the gateway, such that the E_b/N_0 of the access link can be known in advance when selecting the MCS of the NB-IoT frame. By doing so, it would be possible to enlarge the end-end throughput. In all cases, the IoT terminal would receive the data in NB-IoT signalling format. Note that all required modifications of case 2) and 3) for increasing the throughput would be transparent to the

 doi:10.20944/preprints202103.0642.v1

IoT terminal, since the time-packing signalling, NB-IoT regeneration and the DVB-S2(X) encapsulation would be conducted at the satellite level.

Finally, as a future research line, it is interesting to study the viability of using time-packing techniques as a potential physical layer security scheme since the self-interference that it introduces by shrinking the pulses could be used as an artificial noise signal to mask the desired information from potential eavesdroppers.

Author Contributions: J. B., and A. D. conceived, designed and analyzed the experiments; J.B. was oriented to DVB-S2(X) and NB-IoT signalling, time-packing generation and its suppression, A.D. channel modeling, J.B. and A.D. wrote the paper

Funding: This research was funded by Agencia Estatal de Investigación (AEI) and the European Regional Development Fund (FEDER) with grant number TERESA- TEC2017-90093-C3-1-R (AEI/FEDER,UE)

Acknowledgments: The authors would like to express their own deepest gratitute to Prof. Càndid Rèig for his support for publishing this paper in this Special Issue.

Conflicts of Interest: The authors declare that there is no personal circumstances or interest that may be perceived as inappropriately influencing the representation or interpretation of reported research results. The funders had no role in the design of the study; in the collection, analyses, or interpretation of data; in the writing of the manuscript, or in the decision to publish the results.

Abbreviations

The following abbreviations are used in this manuscript:

BLER	BLock Error Rate
DVB-S2	Digital Video Broadcasting Second Generation Satellite
DVB-S2X	Digital Video Broadcasting Second Generation Extension
FSO	Free Space Optical
GEO	Geostationary Earth Orbit
HTS	High Throughput Satellites
IM/DD	Intensity Modulation / Decision Detection
MCS	Modulation and Coding Scheme
NOMA	Non Orthogonal Multiple Acces
NPBCH	Narrowband Physical Broadcast Channel
NPDCCH	Narrowband Physical Downlink Control Channel
NPDSCH	Narrowband Physical Downlink Shared Channel
NPSS	Narrowband Primary Synchronization Signal
NSSS	Narrowband Secondary Synchronization Signal
NB-IoT	Narrow-Band Internet of Things
OFDM	Orthogonal Frequency Division Multiplexing
OTA	Over-The-Air
PAM	Pulse Amplitude Modulation
QPSK	Quadrature Pulse Shift Keying
THR	Throughput

1. Research, N.S. M2M and IoT via Satellite **2019**.
2. CISCO. CISCO Annual Internet Report. White paper, CISCO, 2018.
3. VIASAT. Available on: https://www.viasat.com/products/high-capacity-satellites **2020**.
4. Telesat. Available. http://www.telesat.com/services/leo **2020**.
5. Mata-Calvo, R.; Giggenbach, D.; Le Pera, A.; Poliak, J.; Barrios, R.; Dimitrov, S. Optical feeder links for very high throughput satellites–System perspectives. Proc. Ka Broadband Commun., Navigation and Earth Observation Conf., 2015, pp. 1–7.
6. Dimitrov, S.; Matuz, B.; Liva, G.; Barrios, R.; Mata-Calvo, R.; Giggenbach, D. Digital modulation and coding for satellite optical feeder links. Proc. Advanced Satellite Multimedia Systems Conf. and Signal Process. for Space Commun. Workshop, 2014, pp. 150–157.

7. Dowhuszko, A.; Mengali, A.; Arapoglou, P.; Pérez-Neira, A. Total degradation of a DVB-S2 satellite system with analog transparent optical feeder link. Proc. IEEE Global Commun. Conf., 2019, pp. 1–6.
8. Bas, J.; Dowhuszko, A. Time-Packing as Enabler of Optical Feeder Link Adaptation in High Throughput Satellite Systems. IEEE 5G World Forum (5GWF), 2020, pp. 186–192.
9. Bas, J.; Dowhuszko, A. Linear Time-Packing Detectors for Optical Feeder Link in High Throughput Satellite Systems. Global Congress on Electrical Engineering (GC-ElecEng), 2020, pp. 1–6.
10. Bas, J.; Dowhuszko, A. End-to-end error control coding capability of NB-IoT transmissions in a GEO satellite system with time-packed optical feeder link. *Industrial IoT Technologies and Applications* **2020**, pp. 1–20.
11. 3GPP. LTE; Evolved Universal Terrestrial Radio Access (E-UTRA); Physical channels and modulation (3GPP TS 36.211 version 16.4.0 Release 16). Technical Report TS 36.211, 2021. Rel. 16.4.
12. 3GPP. Technical Specification Group Radio Access Network; Evolved Universal Terrestrial Radio Access (E-UTRA); Physical layer procedures. Technical Report TS 36.213, 2020. Rel. 16.1.
13. 3GPP. Technical Specification Group Radio Access Network; Evolved Universal Terrestrial Radio Access (E-UTRA); Multiplexing and channel coding. Technical Report TS 36.212, 2021. Rel. 16.4.
14. 3GPP. LTE; Evolved Universal Terrestrial Radio Access (E-UTRA) and Evolved Universal Terrestrial Radio Access Network (E-UTRAN); Overall description; Stage 2. Technical Report TS 36.300, 2021. Rel. 16.4.
15. A.Mody.; E.Gonzalez. An Operator's View: The Medium-Term Feasibility of an Optical Feeder Link for VHTS. *In Proc. Of IEEE International Conference on Space Optical Systems and Applications (ICSO).* **2017**.
16. 3GPP. 3rd Generation Partnership Project; Technical Specification Group Radio Access Network; Study on New Radio (NR) to support non-terrestrial networks (Release 15). Technical Report TR 38.811, 2020. Rel. 15.
17. ETSI. Digital VidSecond generation framodulation Interactive Seother broadbPart 2: DVBEUROPEAN STANDARD N 302 307-2 V1.1.1ideo Broadcasting (DVB);framing structure, channel con systems for Broadcasting, Services, News Gathering anddband satellite applications; DVB-S2 Extensions (DVB-S2X). *ETSI,EN 302 307-2, Ver. 1.1.1* **2014**.
18. Forney, G. Maximum-likelihood sequence estimation of digital sequences in the presence of intersymbol interference. *IEEE Trans. Inform. Theory* **1972**, *18*, 363–378.
19. Viterbi, A. Error bounds for convolutional codes and an asymptotically optimum decoding algorithm. *IEEE Trans. Inform. Theory* **1967**, *13*, 260–269.
20. Hailu, S.; Dowhuszko, A.; Tirkkonen, O. Adaptive co-primary shared access between co-located radio access networks. Proc. Int. Conf. Cognitive Radio Oriented Wireless Netw. and Commun., 2014, pp. 131–135.
21. Kaushal, H.; Kaddoum, G. Optical Communication in Space: Challenges and Mitigation Techniques. *IEEE Commun. Surv. & Tut.* **2017**, *19*, 57–96.
22. Rouissat, M.; Borsali, A.; Chikh-Bled, M. Free space optical channel characterization and modeling with focus on algeria weather conditions. *Int. J. Computer Netw. Inform. Security* **2012**, *4*, 17–23.
23. Willebrand, H.; Ghuman, B. *Free Space Optics: Enabling Optical Connectivity in Today's Networks*; Sams: USA, 2001.
24. Mahalati, R.N.; Kahn, J.M. Effect of fog on free-space optical links employing imaging receivers. *Opt. Express* **2012**, *20*, 1649–1661.
25. Flecker, B.; Gebhart, M.; Leitgeb, E.; Muhammad, S.S.; Chlestil, C. Results of attenuation measurements for optical wireless channels under dense fog conditions regarding different wavelengths. Atmospheric Optical Modeling, Measurement, and Simulation II; Hammel, S.M.; Kohnle, A., Eds. International Society for Optics and Photonics, SPIE, 2006, Vol. 6303, pp. 232–242.
26. Nadeem, F.; Javornik, T.; Leitgeb, E.; Kvicera, V.; Kandus, G. Continental Fog Attenuation Empirical Relationship from Measured Visibility Data. *Radioengineering* **2010**, *19*, 596–600.
27. Vavoulas, A.; Sandalidis, H.G.; Varoutas, D. Weather effects on FSO network connectivity. *IEEE/OSA Journal of Optical Communications and Networking* **2012**, *4*, 734–740.
28. Andrews, L.; Phillips, R. *Laser Beam Propagation Through Random Media*; SPIE Press: Bellingham, WA, USA, 2005.
29. Andrews, L.C.; Phillips, R.L.; Sasiela, R.J.; Parenti, R.R. Strehl ratio and scintillation theory for uplink Gaussian-beam waves: beam wander effects. *Optical Engineering* **2006**, *45*, 1 – 12.

 doi:10.20944/preprints202103.0642.v1

30. Tyson, R.K.; Fraizer, B.W. *Field Guide to Adaptive Optics*; SPIE Field Guides, Vol. FG24: Bellingham, WA, USA, 2012.
31. Mengali, A. Optical feeder link satellite systems. In *Link optimization in future generation satellite systems*; PhD Thesis, University of Luxembourg, 2018; chapter 4, pp. 61–86.
32. Perlot, N.; Dreischer, T.; Weinert, C.; Perdigues, J. Optical GEO feeder link design. Future Netw. Mobile Summit, 2012, pp. 1–8.